Original Research

Dapagliflozin-entresto protected kidney from renal hypertension via downregulating cell-stress signaling and upregulating SIRT1/PGC-1α/Mfn2-medicated mitochondrial homeostasis

Sheung-Fat Ko[1], Chih-Chao Yang[2], Pei-Hsun Sung[3,4,5], Ben-Chung Cheng[2], Pei-Lin Shao[6], Yi-Ling Chen[3,4*] and Hon-Kan Yip[3,4,5,6,7,8*]

[1]Department of Radiology, Kaohsiung Chang Gung Memorial Hospital, Kaohsiung 88301; [2]Division of Nephrology, Department of Internal Medicine, Kaohsiung Chang Gung Memorial Hospital, Kaohsiung 88301; [3]Division of Cardiology, Department of Internal Medicine, Kaohsiung Chang Gung Memorial Hospital, Kaohsiung 88301; [4]Institute for Translational Research in Biomedicine, Kaohsiung Chang Gung Memorial Hospital, Kaohsiung 88301; [5]Center for Shockwave Medicine and Tissue Engineering, Kaohsiung Chang Gung Memorial Hospital, Kaohsiung 88301; [6]Department of Nursing, Asia University, Taichung 41354; [7]Department of Medical Research, China Medical University Hospital, China Medical University, Taichung 40402; [8]School of Medicine, College of Medicine, Chang Gung University, Taoyuan 33302

*These authors contributed equally to this paper.

Corresponding authors: Hon-Kan Yip. Email: han.gung@msa.hinet.net; Yi-Ling Chen. Email: rylchen.msu@gmail.com

Impact Statement

Our study provided new insights into the mechanism underlying the preservation of the residual renal function and integrity of kidney parenchyma by dapagliflozin and entresto. The results demonstrated that the 5/6 nephrectomy rat receiving deoxycorticosterone acetate and sodium chloride showed progressive renal failure, as well as a sustained elevated blood pressure for weeks. *In vivo*, dapagliflozin and entresto significantly ameliorated these pathological and histopathological changes in hypertensive kidney disease (HKD) rats. Interestingly, dapagliflozin and entresto significantly downregulated the protein expressions of oxidative stress/mitochondrial-damage/apoptosis/mitochondrial-fission/autophagy/MAPK-family biomarkers, whereas upregulated the protein expressions of mitochondria-biogenesis signaling. Altogether, our findings reported for the first time that dapagliflozin-entresto exerts an additional protective effect against HKD through regulating the SIRT1/PGC-1α-Mfn2 and cell-stress signaling.

Abstract

This study tested whether combined dapagliflozin and entresto would be superior to mere one therapy on protecting the residual renal function and integrity of kidney parenchyma in hypertensive kidney disease (HKD) rat. *In vitro* results showed that the protein expressions of oxidative-stress/mitochondrial-damaged (NOX-1/NOX-2/oxidized-protein/cytosolic-cytochrome-C)/apoptotic (mitochondrial-Bax/cleaved caspeases 3, 9)/cell-stress (p-ERK/p-JNK/p-p38) biomarkers were significantly increased in H_2O_2-treated NRK-52E cells than those of controls that were reversed by dapagliflozin or entresto treatment. Adult-male SD rats ($n=50$) were equally categorized into group 1 (sham-operated-control), group 2 (HKD by 5/6 nephrectomy + DOCA-salt/25 mg/kg/subcutaneous injection/twice weekly), group 3 (HKD + dapagliflozin/orally, 20 mg/kg/day for 4 weeks since day 7 after HKD induction), group 4 (HKD + entresto/orally, 100 mg/kg/day for 4 weeks since day 7 after HKD induction), and group 5 (HKD + dapagliflozin + entresto/the procedure and treatment strategy were identical to groups 2/3/4). By day 35, circulatory levels of blood-urine-nitrogen (BUN)/creatinine and urine protein/creatinine ratio were lowest in group 1, highest in group 2, and significantly lower in group 5 than in groups 3/4, but no difference between groups 3/4. Histopathological findings showed the kidney injury score/fibrotic area/cellular expressions of oxidative-stress/kidney-injury-molecule (8-OHdG+/KIM-1+) exhibited an identical trend, whereas the cellular expressions of podocyte components (synaptopodin/ZO-1/E-cadherin) exhibited an opposite pattern of BUN level among the groups. The protein expressions of oxidative stress/mitochondrial-damaged (NOX-1/NOX-2/oxidized protein/cytosolic-cytochrome-C/cyclophilin-D)/apoptotic (mitochondrial-Bax/cleaved-caspase 3)/mitochondrial-fission (PINK1/Parkin/p-DRP1)/autophagic (LC3BII/LC3BI ratio, Atg5/beclin-1)/MAPK-family (p-ERK/p-JNK/p-p38) biomarkers displayed a similar pattern, whereas the protein expression of mitochondria-biogenesis signaling (SIRT1/PGC-1α-Mfn2/complex I-V) displayed an opposite pattern of BUN among the groups. In conclusion, combined dapagliflozin-entresto therapy offered additional benefits on protecting the residual kidney function and architectural integrity in HKD rat.

Keywords: Chronic kidney disease, hypertension, renal function, dapagliflozin, entresto, kidney ultrastructure

***Experimental Biology and Medicine* 2023; 248: 2421–2439. DOI: 10.1177/15353702231198087**

Introduction

High blood pressure (i.e. hypertension), one of the world's most common human-affected illnesses, is a leading cause of stroke, myocardial infarction, vascular disease, and chronic kidney disease (CKD).[1,2] The epidemiologic and clinical observational studies have shown that hypertension and CKD are commonly linked closely together, called hypertensive kidney disease (HKD).[3,4] Thus, HKD is realized as a medical issue referred to a damage for the kidney due to chronic high blood pressure.[3,4] Of importance is that plentiful data have verified that hypertension is the second leading cause of the end-stage renal disease (ESRD) just behind the causal etiology of diabetes mellitus worldwide.[5–8] Basic researches have clearly clarified that uncontrolled high blood pressure commonly leads to high intraglomerular pressure, impairing glomerular filtration which, in turn, deteriorates kidney function and integrity of kidney macro- and micro-structures,[9–11] resulting in progressively hypertensive nephrosclerosis. However, progressive decline in kidney function can adversely lead to worsening control of blood pressure (BP), that is, hypertension and CKD are two sides of the same coin and always mutually affect each other (i.e. called a destructive combination of hypertension-renal syndrome),[12] ultimately progressing from CKD to ESRD.[8,9,13] The clinical symptoms of HKD are often observed when hypertension is present over a decade or longer.[14,15] The earliest clinical manifestations are increased nocturia and induced onset of proteinuria.[16,17] Unfortunately, when abnormal results of routine biochemical tests are identified, severe HKD lesions may have formed. Even more unfortunate is that when the HKD lesions already developed, every aggressive treatment would be futile for the patients. Accordingly, to find an innovative treatment could be of the utmost importance.

Sodium-glucose cotransporter-2 (SGLT-2) is almost exclusively expressed within proximal renal tubule and accounts for about 90% of glucose reabsorption from the tubular fluid (from the nephron). Blocking SGLT-2 reduces glucose uptake into circulation by blocking glucose and sodium reabsorption from renal tubules, thereby causing urinary glucose excretion.[18] Dapagliflozin (DAPA) which is a highly potent, reversible, and selective SGLT-2 inhibitor has been accepted worldwide for the treatment of type 2 diabetes mellitus.[19,20] Intriguingly, abundant evidence has demonstrated that DAPA has a pleiotropic effect beyond hyperglycemic control that includes reduction of fluid volume and BP, vasodilation, decrease in intraglomerular pressure, and improvement of endothelial cell function, heart failure and clinical outcomes regardless of history of coronary artery disease or CKD.[21–27] However, Entresto, a novel drug, consists of the components of the neprilysin inhibitor (sacubitril) and the angiotensin receptor blocker (valsartan).[28] It is a first-in-class angiotensin receptor-neprilysin inhibitor (ARNi) drug for treating patients with heart failure with reduced left ventricular ejection fraction (i.e. HFrEF).[28,29] Abundant data from large randomized, placebo-controlled clinical trials have reported that entresto was superior to angiotensin-converting enzyme inhibitor for improving the congestive symptoms, left ventricular function and clinical outcome in heart failure pati ents.[28,30–35] In addition, growing data from clinical studies have further demonstrated that entresto therapy effectively preserves the renal function in cardiorenal syndrome.[36–38] However, whether combined DAPA and entresto treatment would offer additional benefits on preserving the residual renal function and outcomes in the setting of HKD has not yet been investigated.

Materials and methods

Ethical statement

All animal procedures were approved by the Institute of Animal Care and Use Committee at Kaohsiung Chang Gung Memorial Hospital (Affidavit of Approval of Animal Use Protocol No. 2020062303) and performed in accordance with the Guide for the Care and Use of Laboratory Animals. Animals were housed in an Association for Assessment and Accreditation of Laboratory Animal Care International (AAALAC; Frederick, MD, USA)-approved animal facility in our hospital with controlled temperature and light cycles (24°C and 12/12 light cycle).

MTT cell viability assay

NRK-52E, rat proximal tubule epithelial cells, were obtained from Bioresource Collection and Research Center (#BCRC60086, Hsinchu, Taiwan). NRK-52E were maintained in Dulbecco's Modified Eagle's Medium with 4.5 g/L glucose (#12800-017, Gibco-Thermo Fisher Scientific, Grand Island, NY, USA), 5% fetal bovine serum (#16170-078, Gibco-Thermo Fisher Scientific), and 1% penicillin and 100 μg/mL streptomycin (#15140-122 Gibco-Thermo Fisher Scientific) at 37°C in an atmosphere containing 5% CO_2. For subculture, NRK-52E cells were detached and harvested with 0.25% trypsin-EDTA (#25200-056, Gibco-Thermo Fisher Scientific) in every 2 to 3 days.

To examine whether the concentration of 100 μM of H_2O_2 was optimal for exhibiting a suitable role of oxidative stress on NRK-52E cells and the time courses of cell viability, the MTT assay was conducted for the *in vitro* study. In detail, about 2×10^3 cells in 100 μL of medium (stock in 100% EtOH at 100 mM concentration, working in 1 mM) were seeded into wells of a 96-well plate and incubated for the indicated duration with or without 100 μM H_2O_2. At the end of incubation, MTT solution was added into each well. After incubation, the purple crystal sediment was dissolved in dimethyl sulfoxide (DMSO) and read at 540 nm in an enzyme-linked immunosorbent assay (ELISA) reader. The absorbance value was used to represent the cell number.

Animal model of CKD induction

Pathogen-free, adult male Sprague–Dawley (SD) rats ($n = 50$) weighing 320–350 g (Charles River Technology, BioLASCO Taiwan Co. Ltd., Taiwan) were utilized in this study. The procedure and protocol of CKD induction have been reported by our previous study.[39] In detail, all animals were anesthetized by inhalational 2.0% isoflurane, placed supine on a warming pad at 37°C for midline laparotomies. Sham-operated rats received laparotomy only, while CKD animals were induced by right nephrectomy plus arterial ligation of

upper two-third (upper and middle poles) blood supplies of the left kidney, that is, by leaving lower third of lower pole of kidney with normal blood supply. Such a model allowed preservation of limited amount of functioning renal parenchyma and offered a simulation of CKD.

Deoxycorticosterone acetate (DOCA)-salt induced hypertension rat model

The procedure and protocol have been described by our previous study.[17] Briefly, for creating an animal model of HKD, the CKD rats received DOCA-salt (25 mg/kg of body weight in 0.4 mL of dimethylformamide by subcutaneous injection) twice weekly and 1% NaCl in drinking water daily since day 3 after CKD induction, that is, drinking saline for nearly 5 weeks.

Finally, the combination of DOCA treatment (i.e. increased salt intake), kidney mass reduction, and chronic high BP development is defined as HKD animal model.

Animal grouping

The animals were categorized into group 1 (sham-operated control [SC]), group 2 (HKD only), group 3 (HKD + DAPA [20 mg/kg/day] orally for 4 weeks since day 7 after HKD induction), group 4 (HKD + entresto [100 mg/kg/day] orally for 4 weeks since day 7 after HKD induction), and group 5 (HKD + DAPA + entresto/the procedure and treatment strategy were identical to groups 2, 3, and 4).

The dosages of entresto and dapagliflozin utilized in this study were based on our previous[40] and recent study,[41] respectively.

Animals in each group were euthanized by day 35 after CKD induction, and the kidney in each animal was harvested for individual study after 5% isoflurane inhalation. The kidney specimens were carefully collected for Western blot analysis, immunohistochemical (IHC), and immunofluorescent (IF) stains and HE stain, respectively.

Assessment of right femoral arterial blood pressure (RFABP) by day 35 after HKD induction

The procedure and protocol have been reported by our previous study.[40] In detail, on day 35 after CKD induction, the SD rats in all groups were anesthetized with inhalational 2.0% isoflurane. A sterile 20-gauge, soft plastic needle was inserted into the RFABP. The pressure signals were first transmitted to pressure transducers (UFI, model 1050, CA, USA) and then exported to a bridge amplifier (ML866 PowerLab 4/30 Data Acquisition Systems; ADInstruments Pty Ltd., Castle Hill, NSW, Australia) where the signals were amplified and digitized. The parameters were recorded and later analyzed with the LabChart software (ADInstruments).

To assess the time courses of circulatory levels of blood urine nitrogen (BUN) and creatinine

To determine whether the animal model of HKD was successfully created and the treatment strategies were effective, blood samples were serially collected from vein into BD Vacutainer Rapid Serum Tube (Becton, Dickinson and Company, Franklin Lakes, NJ, USA) before and after the HKD procedure (i.e. prior to and at days 7 and 35 after HKD induction). Concentrations of serum creatinine and BUN were measured using standard laboratory equipment.

Collection of 24-h urine for assessment of the ratio of urine protein to urine creatinine

The procedure and protocol for collection of 24-h urine for determining the ratio of urine protein to creatinine ($R^{uPr/uCr}$) have been described in our previous reports.[39,42] In detail, each animal was put into a metabolic cage (DXL-D, space: 190 × 290 × 550, Suzhou Fengshi Laboratory Animal Equipment Co. Ltd., China) for 24 h with free access to food and water. Urine in 24 h was collected for all animals at baseline and at day 35 after the CKD induction procedure.

Assessment of kidney injury score at day 35 after HKD induction

In detail, the histopathologic scoring of kidney injury was determined in a blinded fashion as our previous studies.[39,42] Briefly, kidney specimens from all animals were fixed in 10% buffered formalin, embedded in paraffin, sectioned at 5 μm and stained with hematoxylin/eosin (HE) staining, Masson's trichrome staining, and Picro sirius red staining to assess tissue morphology and histopathological injury, and collagen fibers for light microscopy. The scoring system reflected the grading of tubular necrosis, loss of brush border, cast formation, Bowman's capsule and tubular dilatation in 10 randomly chosen, non-overlapping fields (200×) as follows: 0 (none), 1 (⩽10%), 2 (11–25%), 3 (26–45%), 4 (46–75%), and 5 (⩾76%).

IHC and IF stains

The procedure and protocol for IHC and IF staining have been described in our previous reports.[39,42] For IHC and IF staining, rehydrated paraffin sections were first treated with 3% H_2O_2 and incubated with Immuno-Block reagent (#BSB0040, Bio SB Inc., Santa Barbara, CA, USA) for 30 min at room temperature. Sections were then incubated with primary antibodies specifically against smooth muscle α-actin (α-SMA)(#A2547, 1:400, Sigma-Aldrich, Massachusetts, USA), cytochrome C (#ab13575, 1:500, Abcam, Cambridge, UK), HSP60 (#ab190828, 1:500, Abcam), E-cadherin (#ab76055, 1:400, Abcam), 8-hydroxy-2-deoxyguanosine (8-OHdG) (#ab62623, 1:500, Abcam), kidney injury molecule (KIM)-1 (#AF3689, 1:400, R&D Systems, Minnesota, USA), synaptopodin (#SC-21537, 1:500, Santa Cruz Biotechnology, Santa Cruz, CA, USA), and zonula occludens-1 (ZO-1) (#ab59720, 1:200, Abcam), followed by incubation with secondary antibodies conjugated with different fluorochromes. IHC analysis was performed using a biotinylated secondary antibody and streptavidin-Horseradish peroxidase (HRP), followed by colorimetric detection using DAB (#CST-010, Cell Signaling Technology) and counterstained with hematoxylin. While sections incubated with the use of irrelevant antibodies served as controls. Three sections of kidney specimen from each rat were analyzed. For quantification, three randomly chosen HPFs (200× or 400× for IHC and IF studies) were analyzed in each section. The mean number of positively stained cells per HPF for each animal was then determined by summation of all numbers divided by 9.

An IHC-based or IF-based scoring system was adopted for semi-quantitative analysis in the kidney as a percentage of positive cells in a blinded fashion (score of positively stained cells for these biomarkers as: 0 = negative staining; 1 = < 15%; 2 = 16–25%; 3 = 26–50%; 4 = 51–75%; 5 = >76%/per HPF).

Flow cytometric assessment for identifying early and late NRK-52E cell apoptosis

The percentages of viable and apoptotic cells were investigated by flow cytometry using double staining of annexin V and propidium iodide (PI) (#556547, BD Pharmingen™ FITC Annexin V Apoptosis Detection Kit I, BD Biosciences, Miami, FL, USA). This is a reproducible method to identify apoptotic cells (i.e. early (annexin V+/PI–) and late (annexin V+/PI+) phases of apoptosis).

Detection of reactive oxygen species

After individual treatments, NRK-52E cells were then loaded with 10 μM of mitoSOX red (#M36008, Molecular Probes-Thermo Fisher Scientific, Eugene, OR, USA), and incubated in the 5% CO2 incubator for 30 min. The cells were washed three times with PBS (#17-517Q, Lonza Bioscience, Basel, Switzerland) and the reactive oxygen species were detected with flow cytometry (excitation/emission: 492–495/517–527 nm).

Western blot analysis

The procedure and protocol for Western blot analysis have been described in our previous reports.[39,42] Briefly, equal amounts (50 μg) of protein extracts were loaded and separated by SDS-PAGE using acrylamide gradients. After electrophoresis, the separated proteins were transferred electrophoretically to a polyvinylidene difluoride (PVDF) membrane (#GE10600023, Sigma-Aldrich Chemie GmbH, Germany). Nonspecific sites were blocked by incubation of the membrane in blocking buffer (5% nonfat dry milk in TBS-T buffer [TBS containing 0.05% Tween 20]) overnight. The membranes were incubated with the indicated primary antibodies (Atg5 (#12994, 1:1000, Cell Signaling Technology, Danvers, MA, USA), mitochondrial Bax (#ab32505, 1: 1000, Abcam), Bcl-2 (#ARG55188, 1:1000, Arigo Biolaboratories, Hsinchu, Taiwan), beclin1 (#3495, 1:1000, Cell Signaling Technology), cleaved caspase 3 (#9665, 1: 1000, Cell Signaling Technology), cleaved caspase 9 (#A22532, 1:1000, ABclonal Science, Inc, Woburn, MA, USA), OXPHOS complex I-V (#ab110413, 1:6000, Abcam), cytochrome C (#536433, 1:2000, BD Biosciences), cyclophilin D (#ab110324, 1:1000, Abcam), phosphorylated (p)-DRP1 (#3455, 1:1000, Cell Signaling Technology), LC3BI/II (#ab48394, 1:2000, Abcam), phosphorylated (p)-ERK1/2 (#442685, 1:1000, Merck Millipore, Burlington, MA, USA), phosphorylated (p)-JNK (#ab112501, 1:1000, Abcam), NOX-1 (#SAB4200097, 1: 1500, Sigma-Aldrich), NOX-2 (#SAB42000118, 1: 1000, Sigma-Aldrich), Mfn2 (#9482, 1:1000, Cell Signaling), phosphorylated (p)-p38 (#M8177, 1:3000, Sigma-Aldrich), Parkin (#ab77924, 1:1000, Abcam), PGC-1(#ab54481, 1:1000, Abcam), and PINK1(#ab23707, 1:1000, Abcam)) for 1 h at room temperature. Horseradish peroxidase-conjugated anti-rabbit immunoglobulin IgG (1:2000, Cell Signaling Technology) was used as a secondary antibody for 1-h incubation at room temperature. The membrane was washed eight times with TBS-T buffer. Immunoreactive bands were visualized by enhanced chemiluminescence (ECL; Amersham Biosciences, Amersham, UK) and exposed to Biomax L film (Kodak, Rochester, NY, USA). For quantification, ECL signals were digitized using Labwork software (UVP, Waltham, MA, USA).

Statistical analysis

Quantitative data were expressed as mean ± SD. Statistical analysis was adequately performed by ANOVA followed by Bonferroni multiple-comparison post hoc test. Statistical analysis was performed using SPSS statistical software for Windows version 22 (SPSS for Windows, version 22; SPSS, IL, USA). A value of $P < 0.05$ was considered as statistically significant.

Results

Cell viability, protein expressions of MAPK family signaling and mitochondrial damaged marker and apoptosis in NRK-52E cells undergoing H_2O_2 treatment (Figure 1)

To test whether the dose of H_2O_2 (100 μM) was optimal for playing the role of oxidative stress, the NRK-52E cells were categorized into NRK-52E only and H_2O_2-treated NRK-52E. The results of cell viability at time points of 24, 48, and 72 h were significantly suppressed in the H_2O_2-treated NRK-52E as compared with NRK-52E only, implicating that such a concentration of H_2O_2 was suitable for the following *in vitro* studies (Figure 1(A) to (C)).

To verify the oxidative-stress regulated MAPK family signaling played a crucial role on cell death, the NRK-52E cells were categorized into G1 (NRK-52E cells only), G2 (NRK-52E cells + H_2O_2 [100 μM] co-cultured for 6 h, followed by washing and continuously cultured for 48 h), G3 (NRK-52E cells + H_2O_2 [100 μM] co-cultured for 6 h, followed by washing and adding DAPA [50 μM] co-cultured for 48 h), and G4 (NRK-52E + H_2O_2 [100 μM] co-cultured for 6 h, followed by washing and adding sacubitril/valsartan [12.5 μM] [i.e. the component of entresto] co-cultured for 48 h), respectively. The result showed that the protein expressions of cytochrome C, an indicator of mitochondrial damage, and cleaved caspase 9, an index of apoptosis, were significantly higher in G2 than in other groups and significantly lower in G1 than G3 and G4, but they showed no difference between G3 and G4, whereas the protein expression of mitochondrial cytochrome showed an opposite pattern of cytosolic cytochrome C among the groups (Figure 1(G) to (I)). However, the protein expressions of p-ERK1/2, p-JNK and p-p38, three indicators of MAPK family, exhibited an identical pattern of apoptotic marker among the four groups (Figure 1(D) to (F)).

To verify the cellular levels of apoptosis, the flow cytometric analysis was utilized in the *in vitro* study. The result demonstrated that the early and late apoptosis were lowest in G1, highest in G2 and significantly lower in G4 than in G3 (Figure 1(J) to (N)).

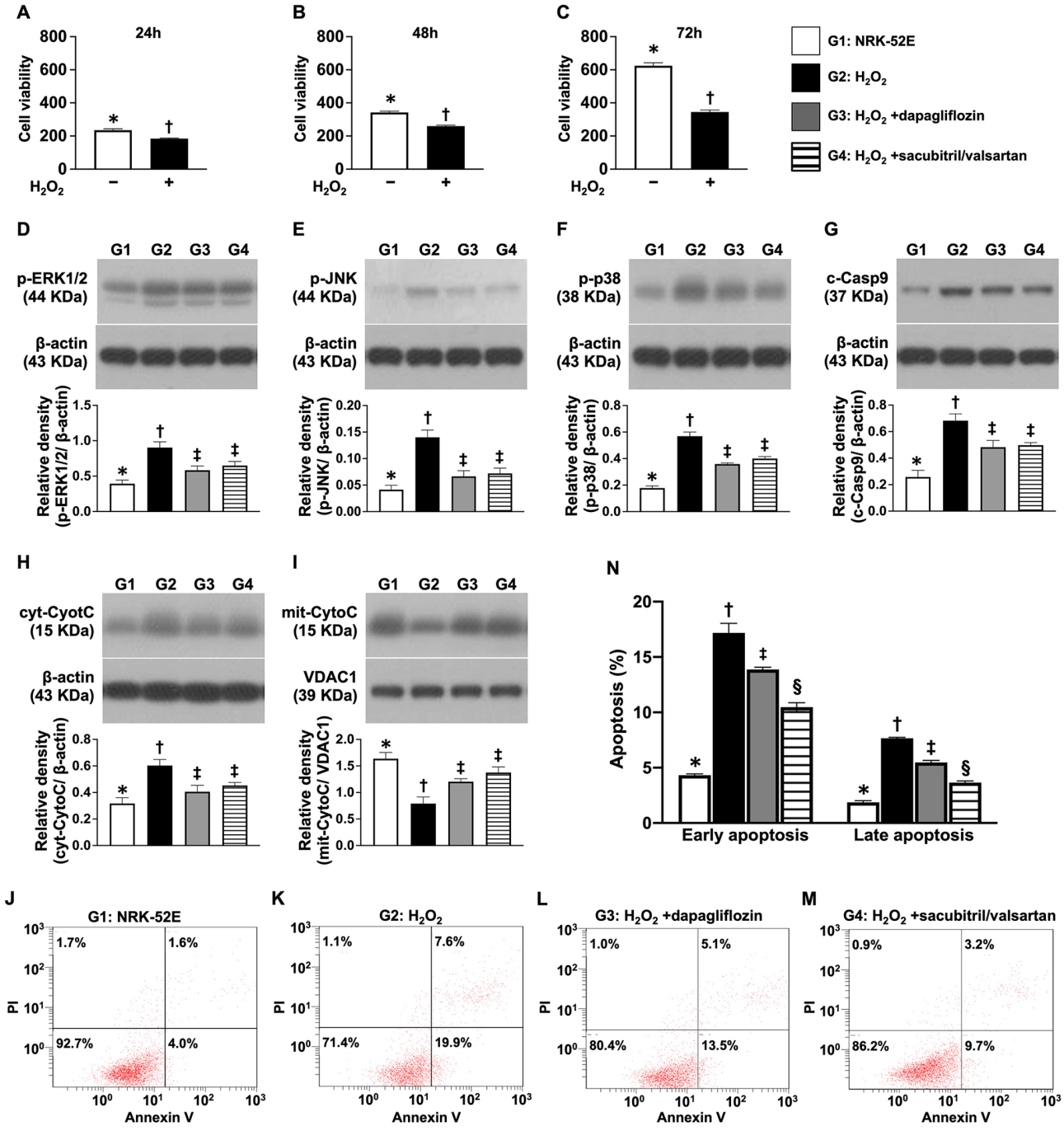

Figure 1. Cell viability and protein expressions of MAPK family signaling, apoptosis and cytochrome C in cytosol and mitochondria and flow cytometric analysis for identification of early and late apoptosis. (A) Cell viability by 24 h, * versus †, $P < 0.001$. (B) Cell viability by 48 h, * versus †, $P < 0.001$. (C) Cell viability by 72 h, * versus †, $P < 0.001$. $n = 6$ for each group (i.e. A to C). (D) Protein expression of phosphorylated (p)-ERK1/2, * versus other group with different symbols (†, ‡), $P < 0.001$. (E) Protein expression of p-JNK, * versus other group with different symbols (†, ‡), $P < 0.001$. (F) Protein expression of p-p38, * versus other group with different symbols (†, ‡), $P < 0.001$. (G) Protein expression of cleaved caspase 9 (c-Casp9), * versus other groups with different symbols (†, ‡), $P < 0.001$. (H) Protein expression of cytosolic cytochrome C (cyt-CytoC), * versus other groups with different symbols (†, ‡), $P < 0.001$. (I) Protein expression of mitochondrial cytochrome C (mit-CytoC), * versus other groups with different symbols (†, ‡), $P < 0.001$. $n = 3$ for each group (i.e. D to I). (J to M) Illustrating the flow cytometric analysis for determining the early and late apoptosis. (N) Flow cytometric result of early (AN-V+/PI-) apoptotic cells, * versus other group with different symbols (†, ‡, §), $P < 0.0001$. Flow cytometric result of late (AN-V+/PI+) apoptotic cells, * versus other group with different symbols (†, ‡, §), $P < 0.0001$. $n = 6$ for each group (i.e. J and K). All statistical analyses were performed by one-way ANOVA, followed by Bonferroni multiple comparison post hoc test. Symbols (*, †, ‡) indicate significance for each other (at 0.05 level). G1 = NRK-52E; G2 = NRK-52E cells + H_2O_2; G3 = NRK-52E cells + H_2O_2 + dapagliflozin; G4 = NRK-52E H_2O_2 + sacubitril/valsartan.

Protein expressions of oxidative stress and apoptosis in NRK-52E cells undergoing the two components of oxidative-stress stimulation (Figure 2)

Next, to elucidate whether combined dapagliflozin + sacubitril/valsartan was better than mere one treatment on protecting the NRK-52E cells against two combinations (i.e. p-Cresol (an oxidative-stress compound) + H_2O_2) of oxidative-stress damage, the cells were categorized into G5 (NRK-52E cells only), G6 (NRK-52E cells + H_2O_2 [100 μM] + p-Cresol [50 μM] co-cultured for 48 h), G7 (NRK-52E cells + H_2O_2 [100 μM] + p-Cresol [50 μM] + DAPA [50 μM] co-cultured for 48 h), G8 (NRK-52E + H_2O_2 [100 μM] + p-Cresol

[50 μM] + sacubitril/valsartan [12.5 μM] co-cultured for 48 h) and G9 (NRK-52E + H_2O_2 + p-Cresol + combined DAPA and sacubitril/valsartan co-cultured for 48 h), respectively. The western blot analysis demonstrated that the protein expressions of mitochondrial Bax and cleaved caspase 3, two indicators of apoptosis, were lowest in G5, highest in G6 and significantly lower in G9 than in G7 and G8, but they did not differ between G7 and G8 (Figure 2(A) and (B)). In addition, the oxidized protein expression, an indicator of oxidative stress, exhibited an identical pattern of apoptosis among the groups, whereas the protein expressions of NOX-1, NOX-2, and oxidized protein, another three indices of oxidative stress, were lowest in G5, highest in G6, significantly lower in G9 than in G7 and G8, and significantly lower in G8 than G7 (Figure 2(D) to (F)). However, protein expression of Bcl-2, an indicator of anti-apoptosis, displayed an opposite pattern of apoptosis among the groups (Figure 2(C)).

To detect the expression of mitochondrial reactive oxygen species (ROS), the flow cytometric analysis was analyzed, followed by mitoSOX dye staining. As we expected, mean fluorescent intensity of mitoSOX (i.e. indicated the ROS expression) exhibited an identical pattern of mitochondrial Bax among the groups (Figure 2(G)).

Time courses of circulatory levels of BUN and creatinine and $R^{uPr/uCr}$, right femoral arterial blood pressure (RFABP) and kidney injury score by day 35 after CKD induction (Figure 3)

Based on the results of our *in vitro* study, we then designed an HKD animal model to test the therapeutic role of dapagliflozin-entresto on protecting the residual renal function and integrity of kidney parenchyma. At baseline, the circulatory levels of BUN and creatinine and the $R^{uPr/uCr}$ did not differ among the groups 1 (SC), 2 (HKD), 3 (HKD + DAPA), 4 (HKD + entresto), and 5 (HKD + DAPA + entresto). However, by day 35 after CKD induction, these three parameters were lowest in group 1, highest in group 2 and significantly higher in groups 3 and 4 than in group 5, but they did not differ between groups 3 and 4 (Figure 3(A) to (F)).

By day 35 prior to euthanizing the animals, the RFABP was measured in each group. The result showed that the RFABP was significantly higher in group 2 than in other groups, significantly higher in groups 3 and 4 than in groups 1 and 5 and significantly higher in group 5 than in group 1, but it showed no difference between groups 3 and 4 (Figure 3(G)).

By day 35 after CKD induction, we collected the kidney specimen for histopathological analysis of kidney damage. The result showed that the kidney injury score exhibited an identical pattern of day-35 circulating level of creatinine among the groups (Figure 3(H) to (M)).

Impact of dapagliflozin and entresto on protein levels of oxidative stress, apoptosis and cell-stress/death signaling by day 35 after CKD induction (Figure 4)

To elucidate whether dapagliflozin and entresto therapies would inhibit the oxidative stress and attenuate the apoptosis and fibrosis in kidney parenchyma, Western blot was utilized for this study. The result showed that the protein expressions of NOX-1 and NOX-2, two indicators of oxidative stress, and protein expressions of mitochondrial Bax and cleaved caspase 3, two indicators of apoptosis, were lowest in group 1, highest in group 2 and significantly higher in groups 3 and 4 than in group 5, but they showed no difference between groups 3 and 4, whereas the protein expression of Bcl-2, an indicator of anti-apoptotic biomarker, exhibited opposite pattern of apoptosis among the groups (Figure 4(A) to (E)).

Further, to elucidate whether the protein expressions of cell-stress/death signaling of *in vivo* situation were comparable with those of *in vitro* study, the Western blot analysis was utilized again. The result demonstrated that the protein expressions of p-ERK1/2, p-JNK and p-p38, three cell-stress biomarkers, exhibited a similar pattern of NOX-1, implicating a cellular intrinsic response to the unfavorable environmental stimulation that was attenuated by dapagliflozin-entresto treatment (Figure 4(F) to (H)). Based on our *in vitro* and *in vivo* results, we, therefore, schematically illustrated a proposed underlying mechanism of the crucial role-played by cell-stress signaling on kidney damage in setting of HKD (Figure 5).

Impact of dapagliflozin and entresto on protein expressions of electron transport chain, autophagy, mitochondrial damage, mitophagy regulators and mitochondrial dynamic biogenesis by day 35 after CKD induction (Figures 6 and 7)

It is well known that DOCA-salt induced hypertension, especially in setting of HKD, actively involves in oxidative stress that would in turn induce mitochondrial damage.[43] Hence, to elucidate the impact of dapagliflozin and entresto on regulating the above-mentioned signaling, the Western blot analysis was utilized. The result showed that the protein expressions of complexes I, II, III, and V, the electron transport chain, were highest in group 1, lowest in group 2 and significantly higher in group 5, but they showed no difference between groups 3 and 4 (Figure 6(A) to (D)). In addition, the protein expressions of ratio of LC3B-II/LC3B-I, Atg5 and beclin 1, three indicators of autophagy, exhibited an opposite manner of electron transport chain among the five groups (Figure 6(F) and (G)). Furthermore, the protein expressions of cytosolic cytochrome C, cyclophilin D, and DRP1, three indicators of mitochondrial damaged markers, exhibited a similar pattern of autophagy (Figure 6(H) to (J)), whereas the protein expression of mitochondrial cytochrome C, an indicator of mitochondrial integrity, exhibited an opposite manner of cytosolic cytochrome C among the groups (Figure 7(A)).

Interestingly, when looked at the energy biogenesis and mitochondrial dynamic biomarkers, we found that the protein expression of PGC-1α, a signaling promoting mitochondrial functional recovery, exhibited an identical pattern of mitochondrial cytochrome C among the five groups (Figure 7(B)). In addition, the protein expression of Mfn2 (i.e. an indicator of mitochondrial fusion) exhibited an identical

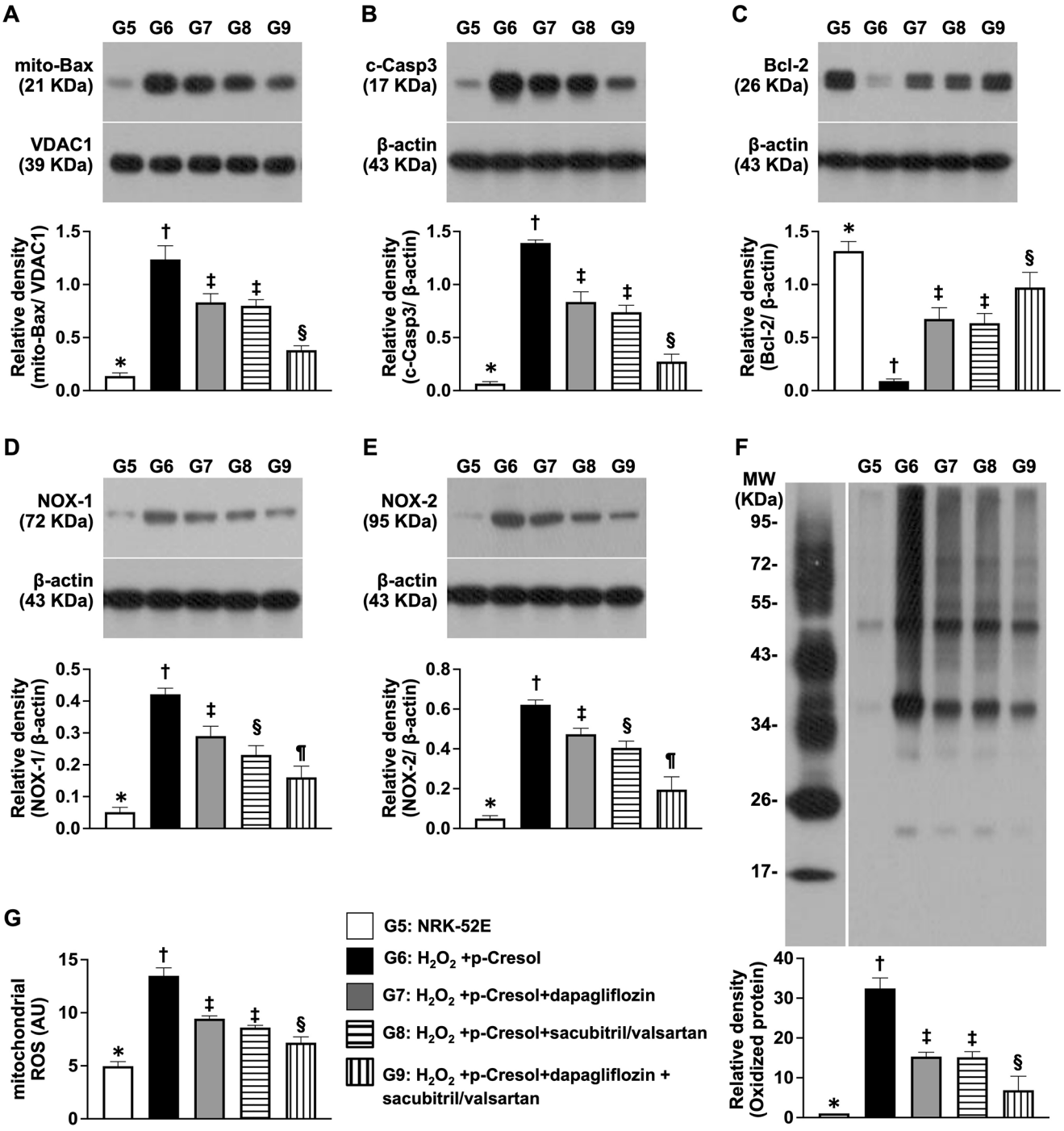

Figure 2. Protein expressions of oxidative stress and apoptosis in NRK-52E cells undergoing the two components of oxidative-stress stimulation. (A) Protein expression of mitochondrial Bax (mit-Bax), * versus other group with different symbols (†, ‡, §), $P < 0.0001$. (B) Protein expression of cleaved caspase 3 (c-Casp3), * versus other group with different symbols (†, ‡, §), $P < 0.0001$. (C) Protein expression of Bcl-2, * versus other group with different symbols (†, ‡, §), $P < 0.0001$. (D) Protein expression of NOX-1, * versus other group with different symbols (†, ‡, §, ¶), $P < 0.0001$. (E) Protein expression of NOX-2, * versus other group with different symbols (†, ‡, §, ¶), $P < 0.0001$. (F) The oxidized protein expression, * versus other groups with different symbols (†, ‡, §), $P < 0.001$ (Note: the left and right lanes shown on the upper panel represent protein molecular weight marker and control oxidized molecular protein standard, respectively.) M.W. = molecular weight; DNP = 1-3 dinitrophenylhydrazone. $n = 3$ for each group (i.e. A to F). (G) Flow cytometric analysis for identification of mitochondrial reactive oxygen species (ROS) (i.e. mean fluorescent intensity of mitoSOX [AU]), * versus other group with different symbols (†, ‡, §), $P < 0.0001$ ($n = 6$ for each group). All statistical analyses were performed by one-way ANOVA, followed by Bonferroni multiple comparison post hoc test. Symbols (*, †, ‡, §) indicate significance for each other (at 0.05 level). G5 (NRK-52E cells only); G6 (NRK-52E cells + H_2O_2 + p-Cresol); G7 (NRK-52E cells + H_2O_2 + p-Cresol + dapagliflozin); G8 (NRK-52E + H_2O_2 + p-Cresol + sacubitril/valsartan); G9 (NRK-52E + H_2O_2 + p-Cresol + combined dapagliflozin; and sacubitril/valsartan).

manner of complex I-IV, whereas the protein expressions of PINK1 and Parkin, two indicators of mitochondrial fission that mediate the mitophagy, exhibited an opposite pattern of Mfn2 among the groups (Figure 7(C) to (E)).

Based on the findings of Figures 6 and 7, we, therefore, schematically illustrated a proposed underlying mechanism of the important roles of oxidative stress/mitochondrial hemostasis signaling on kidney damage in setting of HKD (Figure 5).

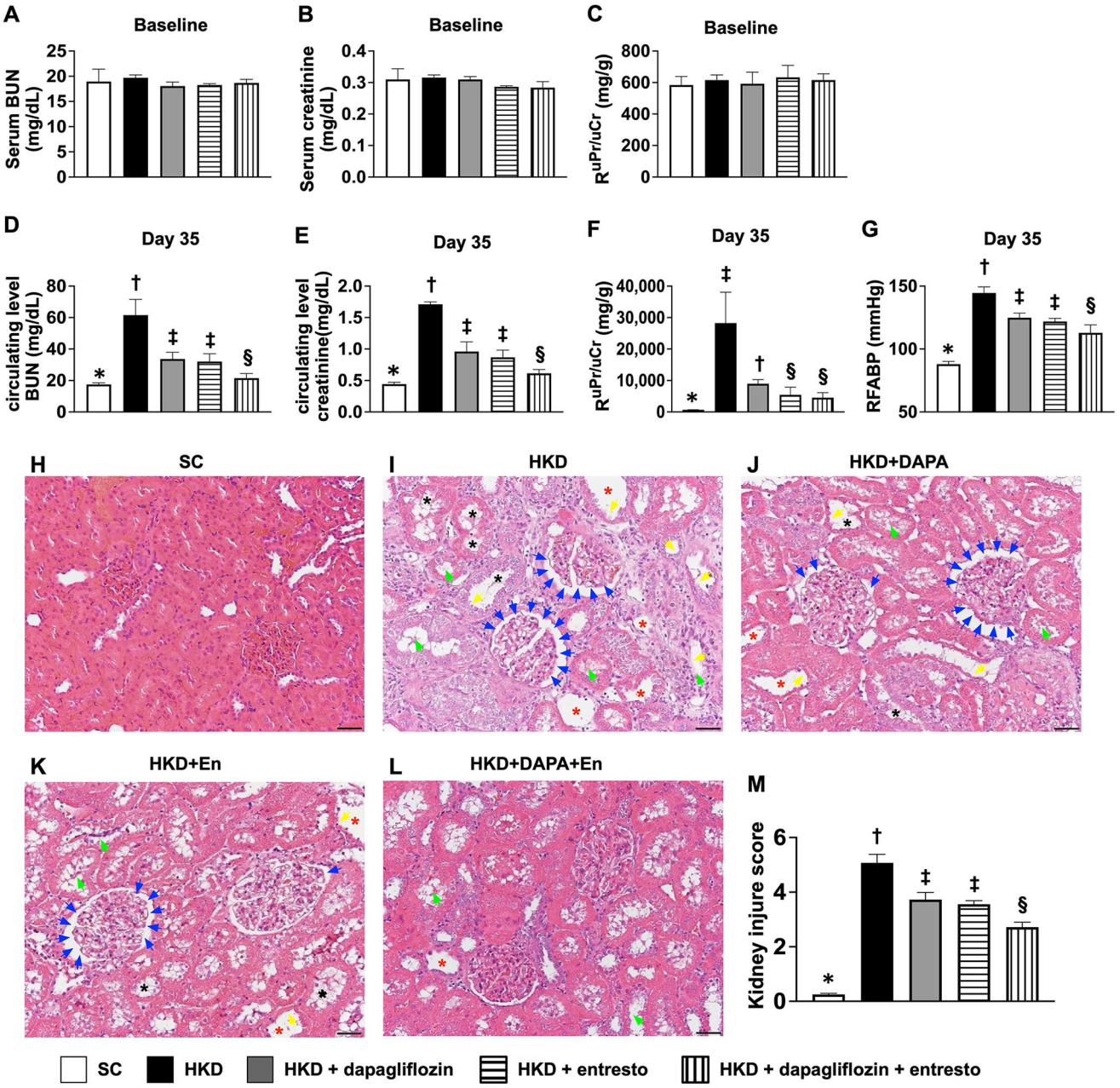

Figure 3. Time courses of circulatory levels of BUN and creatinine and $R^{uPr/uCr}$ and femoral arterial blood pressure and kidney injury score by day 35 after CKD induction. (A to C) Baseline circulating levels of BUN (A) and creatinine (B) and ratio of urine protein to urine creatinine ($R^{uPr/uCr}$) (C) did not differ among the groups, $P > 0.5$. (D to F) By day 35 after CKD induction: circulating levels of BUN (D) and creatinine (E) and $R^{uPr/uCr}$ (F), * versus other groups with different symbols (†, ‡, §), all P values < 0.0001. (G) By day 35 after CKD induction, the right femoral arterial systolic blood pressure (RFASBP), * versus other groups with different symbols (†, ‡, §), $P < 0.0001$. (H to L) Light microscopic findings (200×; H&E stain) showing significantly increased in loss of brush border in renal tubules (yellow arrows), tubular necrosis (green arrows), tubular dilatation (red asterisk), protein cast formation (black asterisk), and dilatation of Bowman's capsule (blue arrows) in CKD group than in other groups. (M) Analytical result of kidney injury score, * versus other group with different symbols (†, ‡, §), $P < 0.0001$. All statistical analyses were performed by one-way ANOVA, followed by Bonferroni multiple comparison post hoc test ($n = 8$ for creatine and BUN level of each group and $n = 6$ for evaluation of kidney injury score each group). Symbols (*, †, ‡, §) indicate significance for each other (at 0.05 level). SC: sham control; HKD: hypertensive kidney disease; DAPA: dapagliflozin; En: entresto.

Impact of dapagliflozin and entresto on cellular levels of fibrosis and collagen deposition by day 35 after CKD induction (Figure 8)

We were also interested in the cellular levels of kidney ultrastructure in setting of HKD, the IHC microscope was utilized in this study. The result demonstrated that fibrotic and collagen-deposition areas were lowest in group 1, highest in group 2 and significantly higher in groups 3 and 4 than in group 5, but they showed no difference between groups 3 and 4, implicating the HKD induced fibrosis and collagen-deposition areas in kidney parenchyma that could be markedly suppressed by dapagliflozin or entresto treatments and even more markedly suppressed by combined dapagliflozin and entresto therapy (Figure 8).

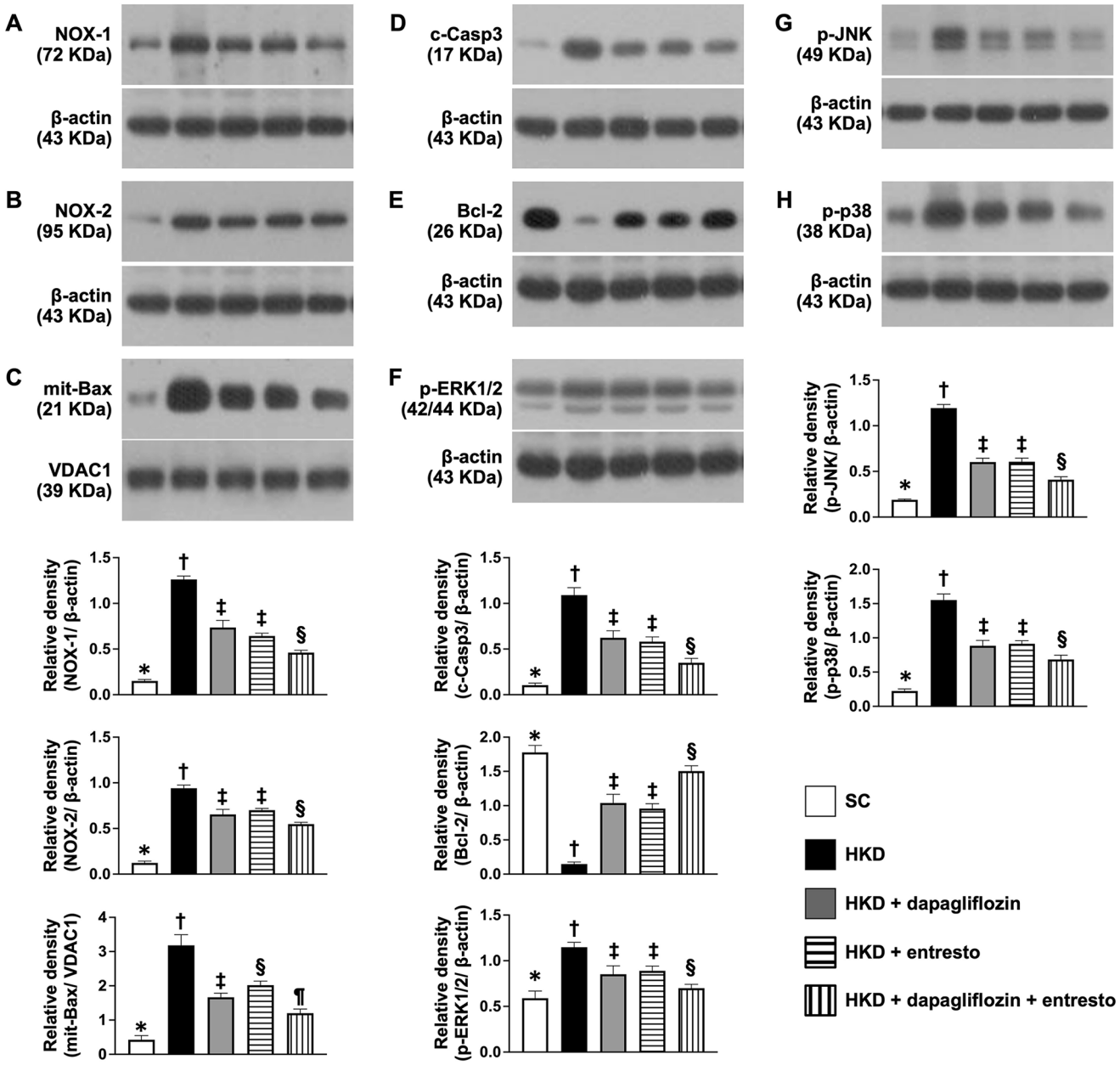

Figure 4. Impact of dapagliflozin and entresto on protein levels of oxidative stress, apoptosis and cell-stress/death signaling by day 35 after CKD induction. (A) Protein expressions of NOX-1, * versus other groups with different symbols (†, ‡, §), $P < 0.0001$. (B) Protein expression of NOX-2, * versus other groups with different symbols (†, ‡, §), $P < 0.0001$. (C) Protein expression of mitochondrial Bax (mit-Bax), * versus other groups with different symbols (†, ‡, §, ¶), $P < 0.0001$. (D) Protein expression of cleaved caspase 3 (c-Casp3), * versus other groups with different symbols (†, ‡, §), $P < 0.0001$. (E) Protein expression of Bcl-2, * versus other groups with different symbols (†, ‡, §), $P < 0.0001$. (F) Protein expression of phosphorylated (p)-ERK1/2, * versus other groups with different symbols (†, ‡, §), $P < 0.0001$. (G) Protein expression of p-JNK, * versus other groups with different symbols (†, ‡, §), $P < 0.0001$. (H) Protein expression of p-p38, * versus other groups with different symbols (†, ‡, §), $P < 0.0001$. All statistical analyses were performed by one-way ANOVA, followed by Bonferroni multiple comparison post hoc test ($n = 6$ for each group). Symbols (*, †, ‡, §, ¶) indicate significance for each other (at 0.05 level). SC: sham control; HKD: hypertensive kidney disease; DAPA: dapagliflozin; En: entresto.

Impact of dapagliflozin and entresto on cell-cell contact component in renal tubules and small vessel density in kidney parenchyma by day 35 after CKD induction (Figure 9)

It is well recognized that the E-cadherin is abundantly expressed in most segments of the nephron for the purpose of maintaining cell-cell adhesion. The result of the present *in vivo* study demonstrated that the cellular expression of E-cadherin (situated predominantly in renal tubular epithelial cells) and number of small vessel (i.e. ⩽25μM) in the kidney parenchyma, were highest in group 1, lowest in group 2 and significantly lower in groups 3 and 4 than in group 5, but they showed no difference between groups 3 and 4 (Figure 9).

Impact of dapagliflozin and entresto on cellular expressions of podocyte components in glomeruli of kidney parenchyma by day 35 after CKD induction (Figure 10)

The link between podocyte damage and proteinuria has been well recognized in CKD setting. To elucidate whether dapagliflozin-entresto therapy would effectively preserve

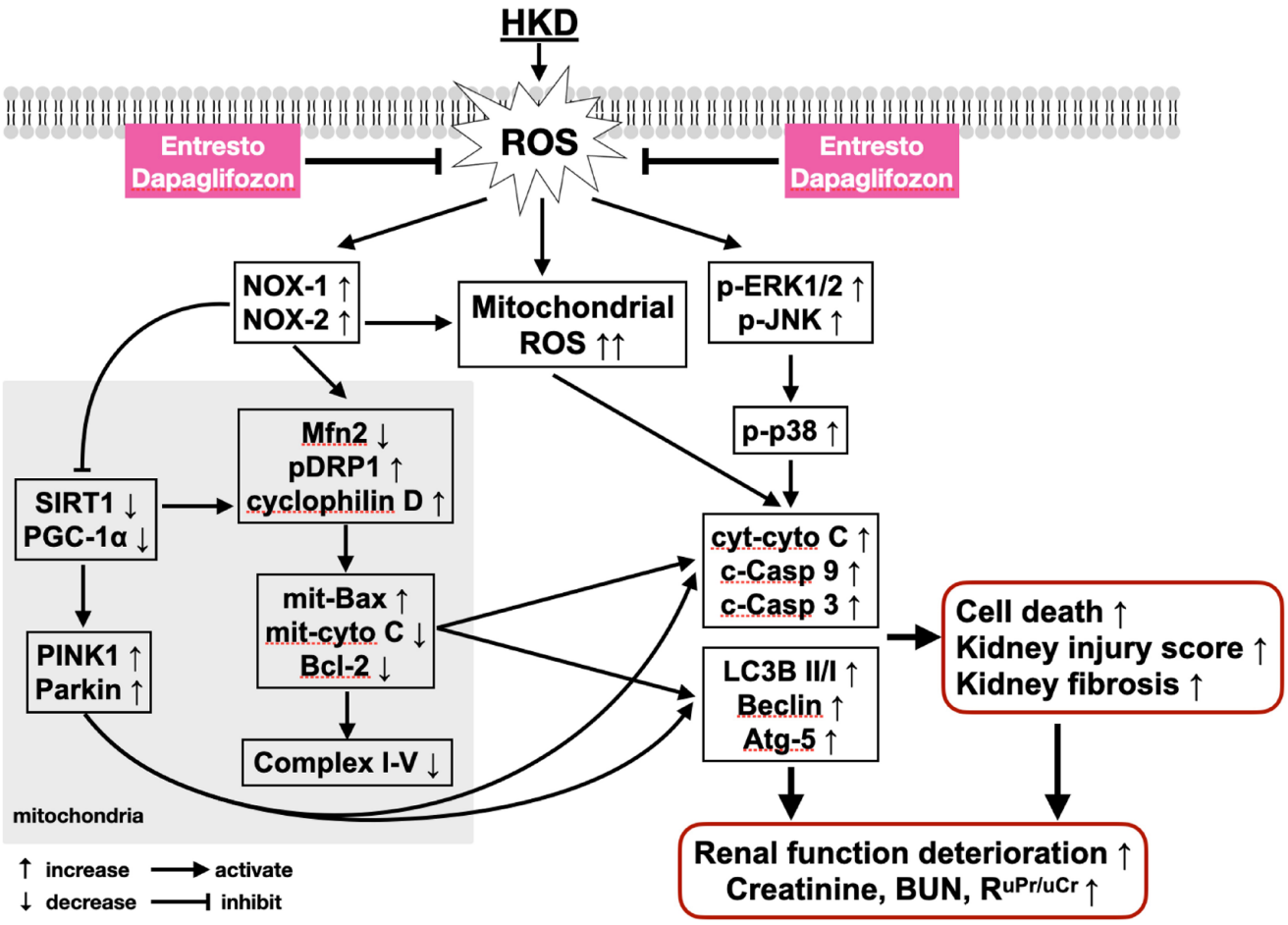

Figure 5. Schematically illustrated the proposed underlying mechanism of DAPA-entresto therapy on protecting the renal tubular cells and integrity of kidney parenchyma against HKD through downregulating oxidative-stress and cell-stress signaling-medicated mitochondrial dynamic hemostasis.

the integrity of the podocyte components, the IF microscope was utilized for the investigation. The result showed that the cellular expressions of ZO-1 and synaptopodin, two podocyte components predominantly located in glomeruli, were highest in group 1, lowest in group 2 and significantly higher in group 5 than in groups 3 and 4, but they were similar in the latter two groups. These findings could explain why the proteinuria was significantly lower in group 3 and 4 and further significantly lower in group 5 as compared with that of group 2 (Figure 10).

Impact of dapagliflozin and entresto on cellular expressions of renal tubular and oxidative DNA damage in kidney parenchyma by day 35 after CKD induction (Figure 11)

It is well-known 8-hydroxy-2′-deoxyguanosine (8-OHdG), a product of oxidative damage to 2′-deoxyguanosine, is well recognized as an essential marker for evaluating oxidative DNA damage. The result of IHC microscopic finding demonstrated that the cellular expression of 8-OHdG, predominantly localized in renal epithelial cells, was lowest in group 1, highest in group 2 and significantly higher in groups 3 and 4 than in group 5, but it showed no difference between groups 3 and 4 (Figure 11(A) to (F)). In addition, the cellular expression of KIM-1, predominantly situated in renal tubules, displayed an identical pattern of 8-OHdG among the groups, implicating that dapagliflozin-entresto therapy effectively protected the renal tubular cells against HKD damage (Figure 11(G) to (L)).

Impact of dapagliflozin and entresto on cellular level of mitochondrial cytochrome C expression of *in vitro* and *in vivo* studies (Figures 12 and 13)

It is well known that as compared with glomerulus cells, the proximal renal tubular cells contain much higher mitochondria for purposes of active transport of glucose, ions, and nutrients. To clarify whether dapagliflozin and entresto treatments would affect the mitochondrial cytochrome C expression, an indicator of integrity of mitochondria, we once again utilized the high-power filed of IF microscopic finding. As we expected, both therapies preserved the integrity of mitochondria in NRK-52E cells (i.e. a rat renal proximal tubular cell line) against the oxidative stress damage (Figure 12). Identically, in the *in vivo* study, we also found that these two therapies protected the mitochondrial integrity in renal tubular cells against the CKD damage (Figure 13).

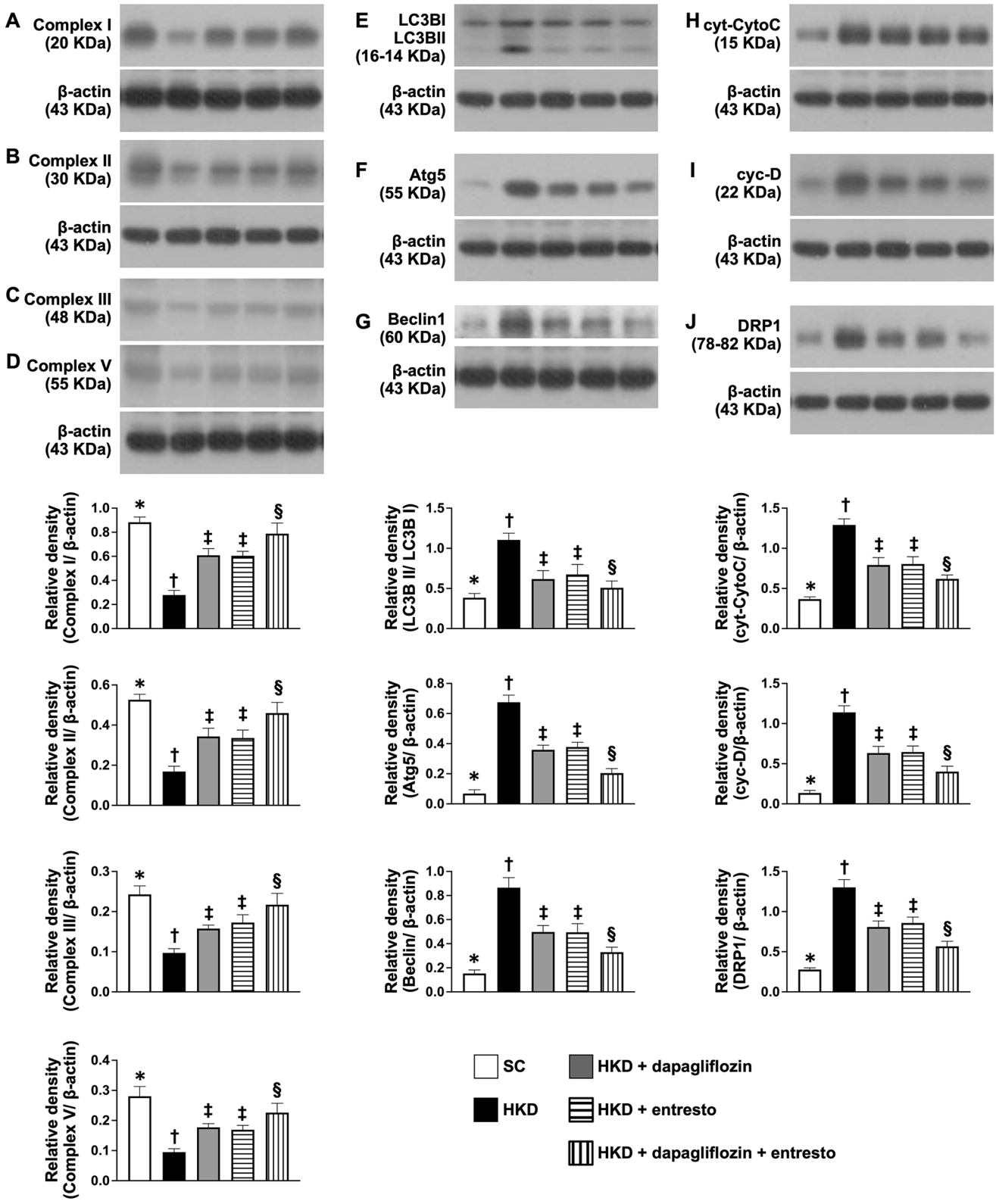

Figure 6. Impact of dapagliflozin and entresto on protein levels of electron transport chain, autophagy, and mitochondrial damage by day 35 after CKD induction. (A) Protein expression of complex I, * versus other groups with different symbols (†, ‡, §), $P < 0.0001$. (B) Protein expression of complex II, * versus other groups with different symbols (†, ‡, §), $P < 0.0001$. (C) Protein expression of complex III, * versus other groups with different symbols (†, ‡, §), $P < 0.0001$. (D) Protein expression of complex V, * versus other groups with different symbols (†, ‡, §), $P < 0.0001$. (E) Protein expressions of ratio of LC3B-II/LC3B-I, * versus other groups with different symbols (†, ‡, §), $P < 0.0001$. (F) Protein expression of Atg5, * versus other groups with different symbols (†, ‡, §), $P < 0.0001$. (G) Protein expression of beclin 1, * versus other groups with different symbols (†, ‡, §), $P < 0.0001$. (H) Protein expression of cytosolic cytochrome C (cyt-CytoC), * versus other groups with different symbols (†, ‡, §), $P < 0.0001$. (I) Protein expression of cyclophilin D (cyc-D), * versus other groups with different symbols (†, ‡, §), $P < 0.0001$. (J) Protein expression of DRP1, * versus other groups with different symbols (†, ‡, §), $P < 0.0001$. All statistical analyses were performed by one-way ANOVA, followed by Bonferroni multiple comparison post hoc test ($n = 6$ for each group). Symbols (*, †, ‡, §) indicate significance for each other (at 0.05 level). SC: sham control; HCKD: hypertensive chronic kidney disease; DAPA: dapagliflozin; En: entresto.

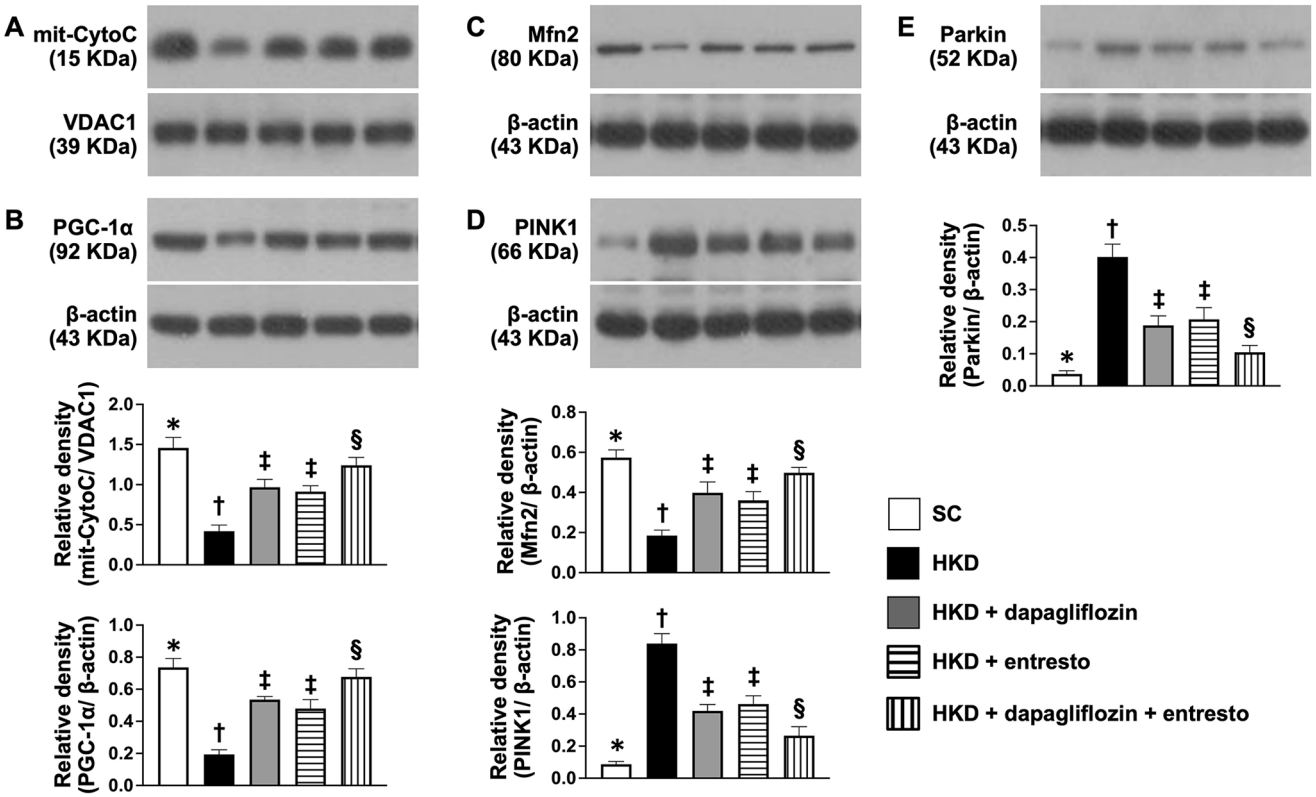

Figure 7. Impact of dapagliflozin and entresto on protein expressions of mitochondrial integrity, mitophagy regulators and mitochondrial dynamic biogenesis by day 35 after CKD induction. (A) Protein expression of mitochondrial cytochrome C (mit-CytoC), * versus other groups with different symbols (†, ‡, §), $P < 0.0001$. (B) Protein expression of protein expressions of PGC-1α, * versus other groups with different symbols (†, ‡, §), $P < 0.0001$. (C) Protein expression of Mfn2, * versus other groups with different symbols (†, ‡, §), $P < 0.0001$. (D) Protein expression of PINK1, * versus other groups with different symbols (†, ‡, §), $P < 0.0001$. (E) Protein expression of Parkin, * versus other groups with different symbols (†, ‡, §), $P < 0.0001$. All statistical analyses were performed by one-way ANOVA, followed by Bonferroni multiple comparison post hoc test ($n = 6$ for each group). Symbols (*, †, ‡, §) indicate significance for each other (at 0.05 level). SC: sham control; HKD: hypertensive kidney disease; DAPA: dapagliflozin; En: entresto.

Discussion

This study exploring the impact of dapagliflozin and entresto therapies on protecting the kidney functional and architectural integrities against HKD damage delivered several striking implications. Frist, dapagliflozin and entresto therapies significantly preserved and these two regimens combined even more significantly preserved residual renal function and ameliorated proteinuria and systolic blood pressure in HKD animals than in those of HKD animals without receiving any treatment. Second, both *in vitro* and *in vivo* studies demonstrated that renal tubular cells which always serve as active transporters (i.e. consume high amount of energy) obtained great benefits from dapagliflozin-entresto treatment through upregulation of Mfn2 (i.e. maintained mitochondrial homeostasis). Third, this study proved that combined dapagliflozin and entresto treatment could offer synergic effect on protecting the kidney functional and parenchymal integrities. Finally, the results of this study (i.e. from both *in vitro* and *in vivo* studies) delineated the underlying mechanism of the initiation and propagation of HKD induced kidney damage and highlighted the most effective therapeutic innovation (referred to Figure 5).

To this day, the preventive treatment of HKD into ESRD is still regrettably an unmet need, suggesting the treatment of HKD to safeguard the kidney for further damage remains a formidable challenge. Interestingly, our recent finding demonstrated that combined dapagliflozin-entresto offered additional benefits on protecting the heart function against ischemia-reperfusion injury.[41] It is well recognized that cardiovascular disease (CVD) and CKD usually share the majority of risk factors, suggesting CVD and CKD are two sides of the same coin. Based on this concept and the findings of our recent report,[41] we therefore designed the current study. The most important finding in this study was that the circulatory BUN and creatinine levels and the $R^{uPr/uCr}$ (i.e. functional integrity) as well as the histopathological findings of ultrastructural feature damage (i.e. kidney injury score and fibrosis) were substantially reduced by dapagliflozin and entresto therapies and more substantially reduced by these two regimens combined in those of HKD animals. In this way, our recent study[41] and the results of this study highlighted the distinctively therapeutic potential of dapagliflozin and entresto, especially when utilization of this combination therapy would offer unexpected benefits for setting of HKD in rat.

An association between increased oxidative-stress and mitochondrial damage has been fully investigated.[44] A principal finding from both *in vitro* and *in vivo* studies was that the oxidative stress (i.e. NOX-1, NOX-2, oxidized protein, and 8-OHdG) and mitochondrial damaged biomarkers (i.e. DRP1, cyclophilin D, and cytosolic cytochrome C) were

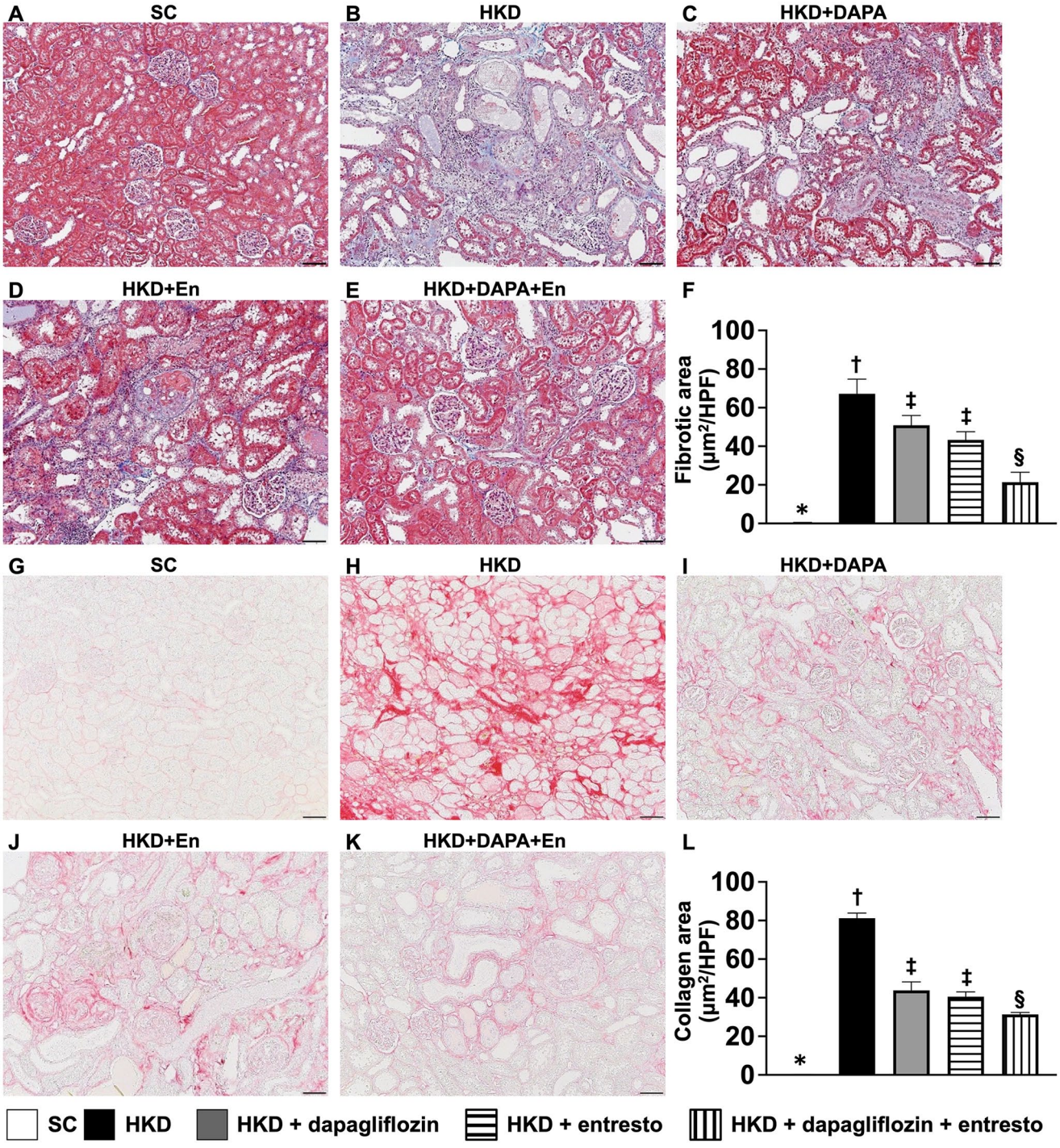

Figure 8. Impact of dapagliflozin and entresto on cellular levels of fibrosis and collagen deposition by day 35 after CKD induction. (A to E) Illustrating the microscopic finding (100×) of Masson's trichrome stain for identification of fibrotic area (blue color). (F) Analytical result of fibrotic area, * versus other group with different symbols (†, ‡, §), $P < 0.0001$. (G to K) Illustrating the microscopic finding (100×) of Sirius red stain for identification of collagen-deposition area (pink). (L) Analytical result of collagen-deposition area, * versus other group with different symbols (†, ‡, §), $P < 0.0001$. Scale bar in right lower corner represents 100μm. All statistical analyses were performed by one-way ANOVA, followed by Bonferroni multiple comparison post hoc test ($n = 6$ for each group). Symbols (*, †, ‡, §) indicate significance for each other (at 0.05 level). SC: sham control; HCKD: hypertensive chronic kidney disease; DAPA: dapagliflozin; En: entresto.

remarkably increased in HKD group as compared with the SC group. These findings could, at least in part, explain why the function and renal parenchyma were notably damaged in HKD group as compared with the SC group.

It is well recognized that PGC-1α participates in energy biogenesis via upregulating the expression of Mfn2 which regulates mitochondrial dynamic homeostasis.[45] Interestingly, a previous study has identified that SIRT1/PGC-1α signaling plays a cardinal role on maintaining mitochondrial functional integrity and increasing mitochondrial biogenesis, resulting in protecting the brain integrity in rat after intracranial hemorrhage.[46] An essential finding in

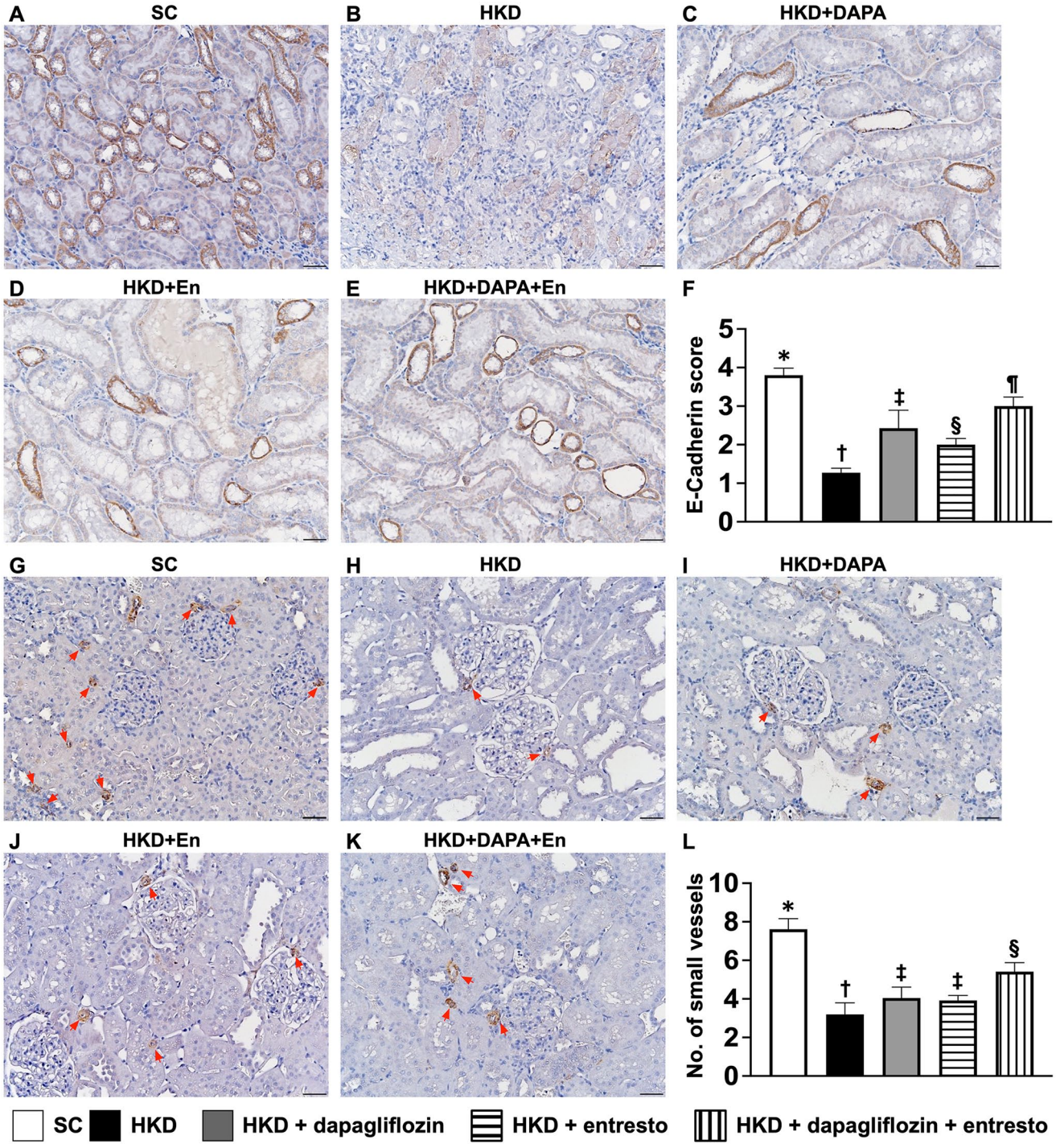

Figure 9. Impact of dapagliflozin and entresto on cell-cell contact component in renal tubules and small vessel density in kidney parenchyma by day 35 after CKD induction. (A to E) Illustrating the microscopic finding (200×) of immunohistochemical (IHC) stain for identification of cellular expression of the E-cadherin (gray color). (F) Analytical result of score expression of E-cadherin, * versus other group with different symbols (†, ‡, §, ¶), $P < 0.0001$. (G to K) Illustrating the microscopic finding (200×) of alpha-smooth muscle actin stain for identification of expression of small vessels (i.e.≤25μM of diameter) (gray color). (L) Analytical result of small number of vessels, * versus other group with different symbols (†, ‡, §), $P < 0.0001$. Scale bar in right lower corner represents 50μm. All statistical analyses were performed by one-way ANOVA, followed by Bonferroni multiple comparison post hoc test ($n = 6$ for each group). Symbols (*, †, ‡, §, ¶) indicate significance for each other (at 0.05 level). SC: sham control; HKD: hypertensive kidney disease; DAPA: dapagliflozin; En: entresto.

this study was that the SIRT1/PGC-1α signaling and Mfn2 biomarker in kidney tissues were remarkably suppressed whereas the biomarkers of PINK1 and Parkin were remarkably increased in HKD group than in SC group. In addition, when looked at the cellular (i.e. NRK-52E cells) expression of mitochondrial cytochrome C, we found that this parameter was markedly depleted by H_2O_2 (i.e. oxidative stress) treatment. Collectively, when inspected expression of mitochondrial cytochrome C in the renal tubular cells in rat kidney, we also observed that this biomarker was remarkably diminished in HKD animals. Our findings proposed that oxidative stress damaged the renal tubular cells and the integrity of

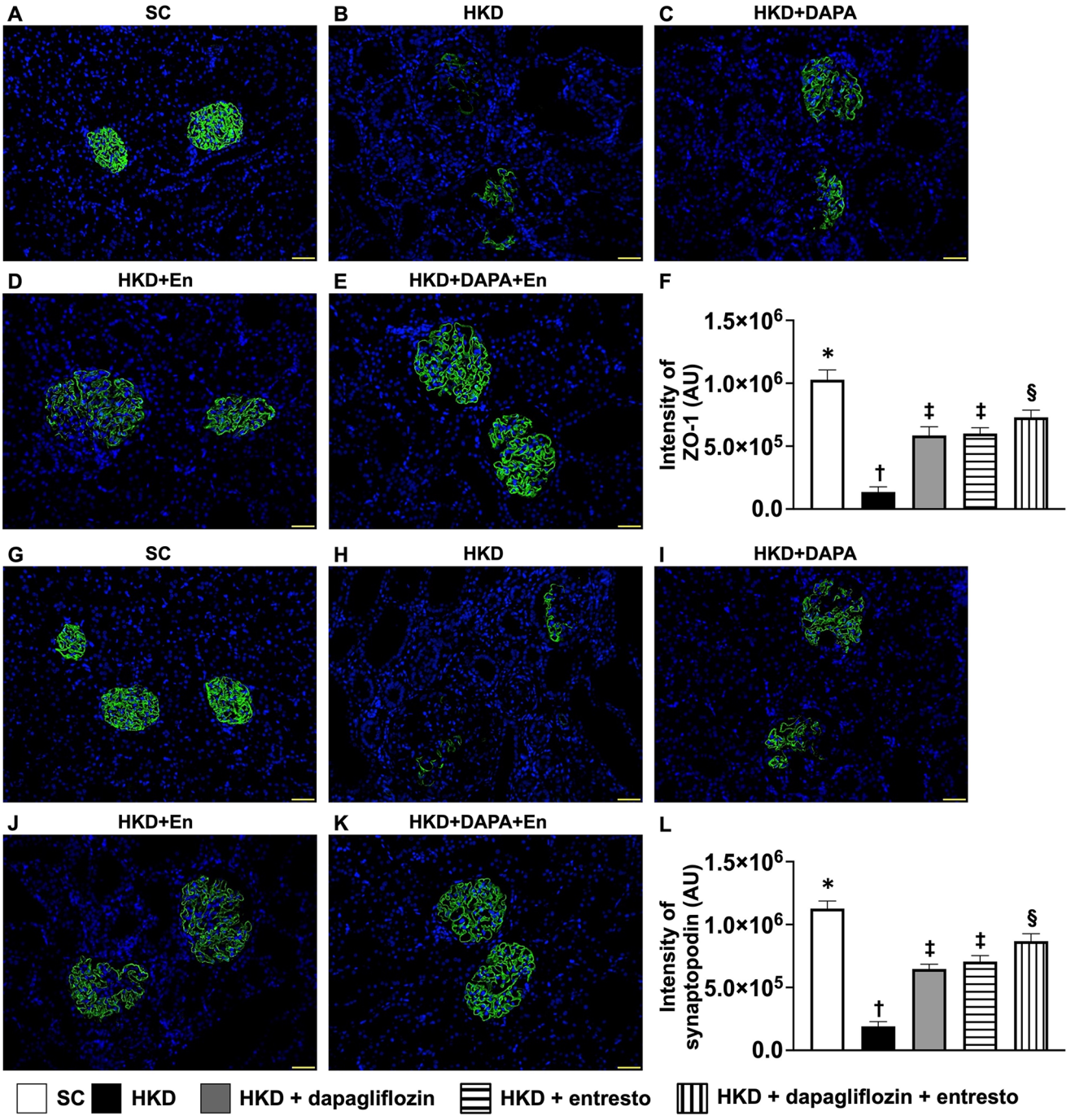

Figure 10. Impact of dapagliflozin and entresto on cellular expressions of podocyte components in glomeruli of kidney parenchyma by day 35 after CKD induction. (A to E) Showing the microscopic finding (200×) of immunofluorescent (IF) stain for identification of cellular expression of ZO-1 (green color). (F) Analytical result of fluorescent intensity of ZO-1, * versus other group with different symbols (†, ‡, §), $P < 0.0001$. (G to K) Showing the IF microscopic finding (200×) for identification of cellular expression of synaptopodin (green color). (L) Analytical result of fluorescent intensity of synaptopodin, * versus other group with different symbols (†, ‡, §), $P < 0.0001$. Scale bar in right lower corner represents 50μm. All statistical analyses were performed by one-way ANOVA, followed by Bonferroni multiple comparison post hoc test ($n = 6$ for each group). Symbols (*, †, ‡, §) indicate significance for each other (at 0.05 level). SC: sham control; HKD: hypertensive kidney disease; DAPA: dapagliflozin; En: entresto.

kidney parenchyma as well as deteriorated the renal function through downregulating the SIRT1/PGC-1α-Mfn2 signaling (referred to Figure 5).

Intriguingly, a lot of previous studies have established that cell-stress signalings are frequently activated in tissue/organ damage in response to ischemia or inflammatory stimulations.[47–49] In addition, an association between upregulation of cell-stress signaling biomarkers and unfavorable outcomes has also been identified by these studies.[47–49] Another essential finding in this study was that the cell-stress biomarkers (i.e. p-ERK1/2, p-JNK, and p-p38) were notably increased in HKD group than in the SC counterpart. Importantly, the apoptotic and autophagic biomarkers were discovered to be concomitantly upregulated with

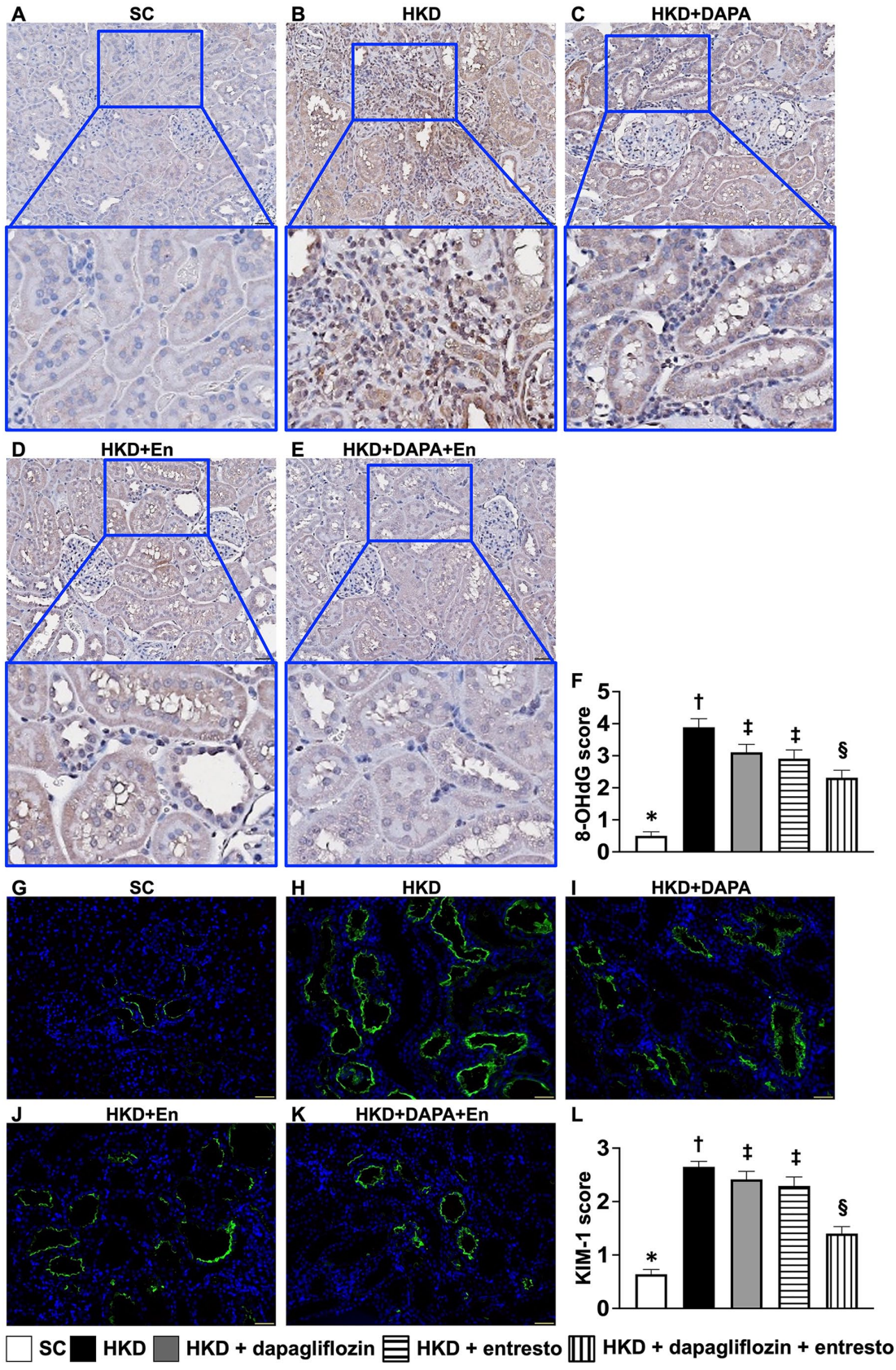

Figure 11. Impact of dapagliflozin and entresto on cellular expressions of renal tubular and oxidative DNA damage in kidney parenchyma by day 35 after CKD induction. (A to E) Illustrating the microscopic finding (200×) for identification of cellular expression of 8-hydroxy-2′-deoxyguanosine (8-OHdG), i.e. an oxidative DNA damage marker (gray color). (F) Analytical result of score expression of 8-OHdG, * versus other group with different symbols (†, ‡, §), $P < 0.0001$. (G to K) Illustrating the immunofluorescent microscopic finding (200×) for identification of cellular expression of kidney injury molecule (KIM)-1. (L) Analytical result of score expression of KIM-1,* versus other group with different symbols (†, ‡, §), $P < 0.0001$. Scale bar in right lower corner represents 50μm. All statistical analyses were performed by one-way ANOVA, followed by Bonferroni multiple comparison post hoc test ($n = 6$ for each group). Symbols (*, †, ‡, §) indicate significance for each other (at 0.05 level). SC: sham control; HKD: hypertensive kidney disease; DAPA: dapagliflozin; En: entresto.

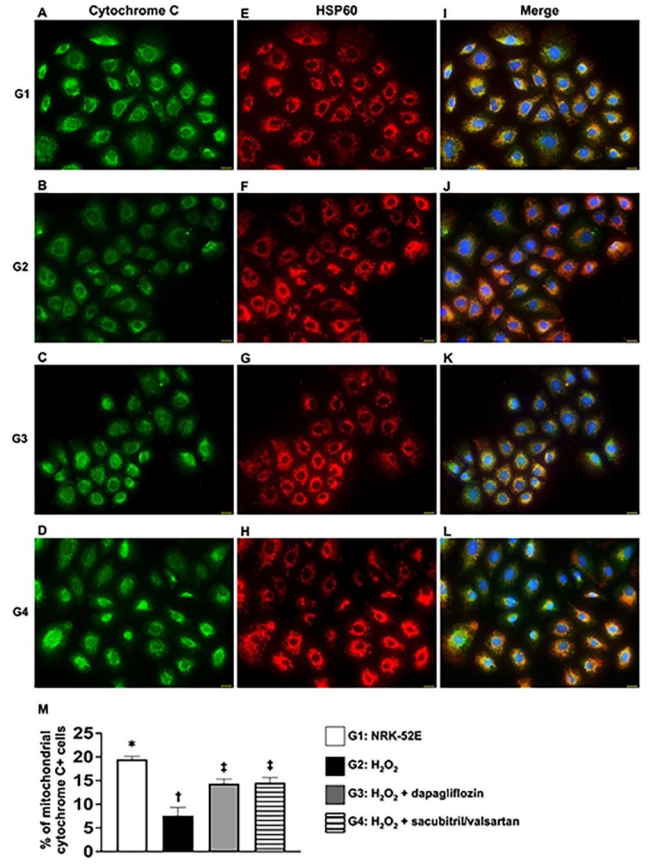

Figure 12. Impact of dapagliflozin and entresto on cellular level of mitochondrial cytochrome C expression in NRK-52E cells. (A to D) Illustrating the immunofluorescent (IF) microscopic finding (400×) for identification of mitochondrial cytochrome C + cells (green color) in NRK-52E cells. (E to H) Illustrating IF microscopic finding (400×) for identification of heat shock protein 60 (HSP60) + cells (red color) in NRK-52E cells. (I to L) Illustrating IF microscopic finding (400×) of merged cytochrome C and HSP60 positively stained cells (i.e. double stain) for identification of cytochrome C in mitochondria (i.e. green-red color). Blue color indicated nuclei stained by DAPI. (M) Analytical result of number of mitochondrial cytochrome C + cells in NRK-52E cells, * versus other group with different symbols (†, ‡), $P < 0.001$. Scale bars in right lower corner represent 20μm. All statistical analyses were performed by one-way ANOVA, followed by Bonferroni multiple comparison post hoc test ($n = 5$ for each group). Symbols (*, †, ‡) indicate significance for each other (at 0.05 level). G1 = NRK-52E; G2 = NRK-52E cells + H_2O_2; G3 = NRK-52E cells + H_2O_2 + dapagliflozin; G4 = NRK-52E H_2O_2 + sacubitril/valsartan.

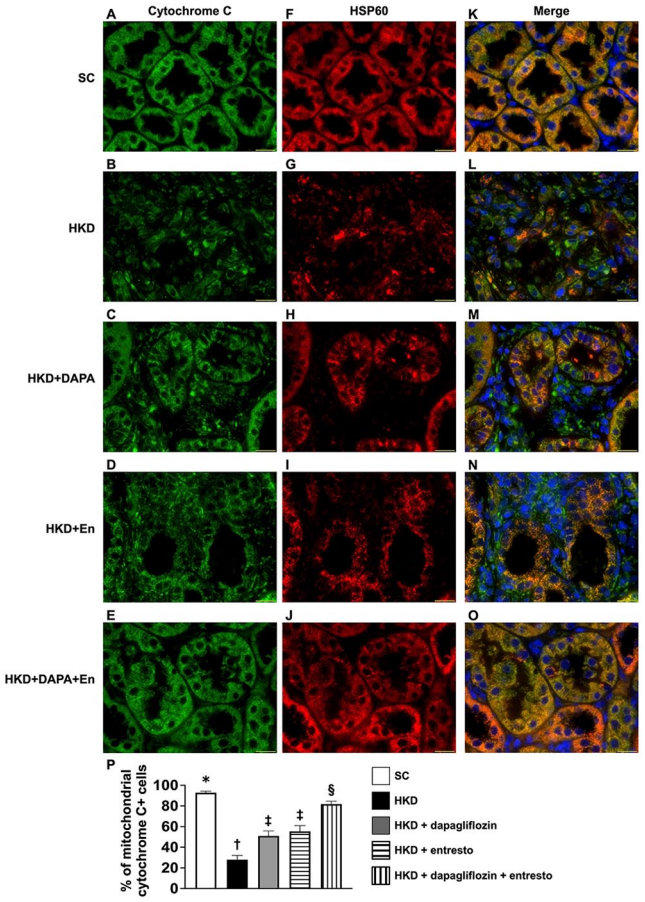

Figure 13. Impact of dapagliflozin and entresto on cellular level of mitochondrial cytochrome C expression in renal tubular cells of rat kidney. (A to E) Illustrating the immunofluorescent (IF) microscopic finding (800×) for identification of mitochondrial cytochrome C + cells (green color) in renal tubular cells. (F to J) Illustrating IF microscopic finding (800×) for identification of heat shock protein 60 (HSP60) + cells (red color) in renal tubular cells. (K to O) Illustrating IF microscopic finding (800×) of merged cytochrome C and HSP60 positively stained cells (i.e. double stain) for identification of cytochrome C in mitochondria (i.e. green-red color). Blue color indicated nuclei stained by DAPI. (P) Analytical result of number of mitochondrial cytochrome C + cells in renal tubular cells, * versus other group with different symbols (†, ‡, §), $P < 0.001$. Scale bars in right lower corner represent 20 μm. All statistical analyses were performed by one-way ANOVA, followed by Bonferroni multiple comparison post hoc test ($n = 6$ for each group). Symbols (*, †, ‡, §) indicate significance for each other (at 0.05 level). All statistical analyses were performed by one-way ANOVA, followed by Bonferroni multiple comparison post hoc test ($n = 6$ for each group). Symbols (*, †, ‡, §) indicate significance for each other (at 0.05 level). SC: sham control; HKD: hypertensive kidney disease; DAPA: dapagliflozin; En: entresto.

those of cell-stress signaling (referred to Figure 5). Our findings, in addition to supporting the findings of the previous reports,[47–49] could partially explain why the renal function and kidney parenchyma were markedly impaired in the former group than in the latter one.

Of paramount important finding in this study was that the above-mentioned perturbations were significantly reversed by dapagliflozin and entresto and further significantly reversed by combined dapagliflozin-entresto treatment, implicating that there could be a synergic effect from this combined regimen. Elaborated so far, the readers would be interested in knowing how the synergic effect is offered by dapagliflozin-entresto on protecting the residual renal function and integrity of kidney architecture. Perhaps, three reasons could be utilized to explain this issue. First, basic research already helps us to understand that angiotensin II type I receptor blockers (ARBs) lead both glomerulus afferent and efferent arteries to dilate, resulting in an increased glomerulus filtration rate. However, this would increase the intra-glomerulus pressure that may pose as a potential risk for glomerulus-apparatus damage in some situations. However, the dapagliflozin therapy would reduce the blood flow into the intra-glomerulus through just right restriction of the afferent artery dilatation, resulting in not only reducing the glomerulus pressure but also keeping an adequate blood flow from intra-glomerulus into the efferent artery. These two drugs which worked complementarily together, called synergic effect, indeed significantly preserved the integrity of podocyte components (i.e. ZO-1, synaptopodin) which could explain why the proteinuria was markedly reduced in HKD after receiving the dapagliflozin-entresto therapy. Second, the pharmacokinetic property of dapagliflozin and entresto comparably attenuates the blood pressure

through vasodilatation and regulation of circulatory B-type Natriuretic Peptide level. These could protect the integrity of kidney parenchyma and could explain why the RFABP was most effectively reduced by the combined dapagliflozin and entresto treatment. Third, physiologically, the proximal and distal renal tubules depend on efficient oxidative capacity to facilitate the active transport of glucose, ions, and nutrients. Therefore, abundance of mitochondria in the distal and proximal tubules is necessary for maintaining the energy demands, making them less susceptible to oxidative-stress damage. Pathologically, such as the setting of HKD, the mitochondrial damage by oxidative stress which in turn would lead to even more damage to renal tubular cells. This distinctively pathological feature could explain why *in vitro* and *in vivo* studies demonstrated that the mitochondrial cytochrome C in renal tubular cells (Figure 11 and 12) and the protein levels of apoptosis (i.e. in index of cell death in both *in vitro* and *in vivo*) and KIM-1 in kidney specimen were markedly reduced in HKD animals. This study has limitations. First, the dosages of dapagliflozin and entresto were not assessed by stepwise increase in concentrations. Thus, this study did not provide detailed information regarding which were the optimal dosages of dapagliflozin-entresto for protecting the kidney against HKD damage. Second, the hypoglycemic effect of dapagliflozin on the renoprotection and benefit of entresto on the cardiac protection was not tested in this study. Thus, we did not know if the synergistic effect of dapagliflozin-entresto on the preservation of renal function and structure came from the two aforementioned mechanisms. Third, currently, there is no large randomized clinical trial testing that whether dapagliflozin or entresto therapy is safe or not for the ESRD patients. Therefore, our HKD animal model which was not a model of ESRD still left the question unanswered.

In conclusion, the results of this study demonstrated dapagliflozin-entresto effectively protected the renal function and the integrity of kidney architecture through regulating the SIRT1/PGC-1α-Mfn2 and cell-stress signaling.

AUTHORS' CONTRIBUTIONS

All authors participated in the design, interpretation of the studies, analysis of the data, and review of the manuscript; SFK was responsible for funding acquisition; SFK, YLC, and HKY designed the study; CCY, BCC, PHS, and PLS conducted the experiments; CCY, BCC, SFK, PLS, PHS, and YLC did formal analysis and data curation. YLC and HKY wrote the manuscript and all named authors contributed revising manuscript.

ACKNOWLEDGEMENTS

The authors thank Dr John Y Chiang for proofreading the article.

DECLARATION OF CONFLICTING INTERESTS

The author(s) declared no potential conflicts of interest with respect to the research, authorship, and/or publication of this article.

FUNDING

The author(s) disclosed receipt of the following financial support for the research, authorship, and/or publication of this article: This work was supported by the Kaohsiung Chang Gung Memorial Hospital, Chang Gung University, Taiwan [CMRPG8K1381]; and the National Science and Technology Council, Taiwan [NMRPG8K6141, NMRPG8K6142, NMRPG8K6143].

ORCID ID

Hon-Kan Yip https://orcid.org/0000-0002-6305-5717

REFERENCES

1. Drozdz D, Kawecka-Jaszcz K. Cardiovascular changes during chronic hypertensive states. *Pediatr Nephrol* 2014;**29**:1507–16
2. Tedla FM, Brar A, Browne R, Brown C. Hypertension in chronic kidney disease: navigating the evidence. *Int J Hypertens* 2011;**2011**:132405
3. Hamrahian SM, Falkner B. Hypertension in chronic kidney disease. *Adv Exp Med Biol* 2017;**956**:307–25
4. Viazzi F, Bonino B, Mirijello A, Fioretto P, Giorda C, Ceriello A, Guida P, Russo GT, De Cosmo S, Pontremoli R, Group AM-AS. Long-term blood pressure variability and development of chronic kidney disease in type 2 diabetes. *J Hypertens* 2019;**37**:805–13
5. Tozawa M, Iseki K, Iseki C, Kinjo K, Ikemiya Y, Takishita S. Blood pressure predicts risk of developing end-stage renal disease in men and women. *Hypertension* 2003;**41**:1341–5
6. Drawz PE, Rosenthal N, Babineau DC, Rahman M. Nighttime hospital blood pressure: a predictor of death, ESRD, and decline in GFR. *Ren Fail* 2010;**32**:1036–43
7. Mills KT, Bundy JD, Kelly TN, Reed JE, Kearney PM, Reynolds K, Chen J, He J. Global disparities of hypertension prevalence and control: a systematic analysis of population-based studies from 90 countries. *Circulation* 2016;**134**:441–50
8. Sumida K, Molnar MZ, Potukuchi PK, Thomas F, Lu JL, Yamagata K, Kalantar-Zadeh K, Kovesdy CP. Pre-end-stage renal disease visit-to-visit systolic blood pressure variability and post-end-stage renal disease mortality in incident dialysis patients. *J Hypertens* 2017;**35**:1816–24
9. Harnett J, Gerber R, Gruben D, Koenig AS, Chen C. Evaluation of real-world experience with tofacitinib compared with adalimumab, etanercept, and abatacept in RA patients with 1 previous biologic DMARD: data from a U.S. *J Manag Care Spec Pharm* 2016;**22**:1457–71
10. Bidani AK, Polichnowski AJ, Loutzenhiser R, Griffin KA. Renal microvascular dysfunction, hypertension and CKD progression. *Curr Opin Nephrol Hypertens* 2013;**22**:1–9
11. Palmer BF, Clegg DJ. Renal considerations in the treatment of hypertension. *Am J Hypertens* 2018;**31**:394–401
12. Griffin KA. Hypertensive kidney injury and the progression of chronic kidney disease. *Hypertension* 2017;**70**:687–94
13. Amraoui F, Bos S, Vogt L, van den Born BJ. Long-term renal outcome in patients with malignant hypertension: a retrospective cohort study. *BMC Nephrol* 2012;**13**:71
14. Duni A, Dounousi E, Pavlakou P, Eleftheriadis T, Liakopoulos V. Hypertension in chronic kidney disease: novel insights. *Curr Hypertens Rev* 2020;**16**:45–54
15. Polychronopoulou E, Wuerzner G, Burnier M. How do I manage hypertension in patients with advanced chronic kidney disease not on dialysis? Perspectives from clinical practice. *Vasc Health Risk Manag* 2021;**17**:1–11
16. Wang XC, Liu CH, Chen YJ, Wu Y, Yang LS, Liu HM, Liao HL. Clinical and pathological analysis of the kidney in patients with hypertensive nephropathy. *Exp Ther Med* 2013;**6**:1243–6
17. Ko SF, Yip HK, Zhen YY, Hung CC, Lee CC, Huang CC, Ng SH, Chen YL, Lin JW. Renal damages in deoxycorticosterone acetate-salt hypertensive rats: assessment with diffusion tensor imaging and T2-mapping. *Mol Imaging Biol* 2020;**22**:94–104
18. Ghezzi C, Loo DDF, Wright EM. Physiology of renal glucose handling via SGLT1, SGLT2 and GLUT2. *Diabetologia* 2018;**61**:2087–97
19. Dhillon S. Dapagliflozin: a review in type 2 diabetes. *Drugs* 2019;**79**:1135–46
20. Fioretto P, Del Prato S, Buse JB, Goldenberg R, Giorgino F, Reyner D, Langkilde AM, Sjöström CD, Sartipy P, DERIVE Study Investigators.

Efficacy and safety of dapagliflozin in patients with type 2 diabetes and moderate renal impairment (chronic kidney disease stage 3A): the DERIVE Study. *Diabetes Obes Metab* 2018;**20**:2532–40
21. Phrommintikul A, Wongcharoen W, Kumfu S, Jaiwongkam T, Gunaparn S, Chattipakorn S, Chattipakorn N. Effects of dapagliflozin vs vildagliptin on cardiometabolic parameters in diabetic patients with coronary artery disease: a randomised study. *Br J Clin Pharmacol* 2019;**85**:1337–47
22. Wiviott SD, Raz I, Bonaca MP, Mosenzon O, Kato ET, Cahn A, Silverman MG, Zelniker TA, Kuder JF, Murphy SA, Bhatt DL, Leiter LA, McGuire DK, Wilding JPH, Ruff CT, Gause-Nilsson IAM, Fredriksson M, Johansson PA, Langkilde AM, Sabatine MS, Investigators D-T. Dapagliflozin and cardiovascular outcomes in type 2 diabetes. *N Engl J Med* 2019;**380**:347–57
23. Zainordin NA, Hatta S, Mohamed Shah FZ, Rahman TA, Ismail N, Ismail Z, Abdul Ghani R. Effects of dapagliflozin on endothelial dysfunction in type 2 diabetes with established ischemic heart disease (EDIFIED). *J Endocr Soc* 2020;**4**:bvz017
24. McMurray JJV, Solomon SD, Inzucchi SE, Kober L, Kosiborod MN, Martinez FA, Ponikowski P, Sabatine MS, Anand IS, Belohlavek J, Bohm M, Chiang CE, Chopra VK, de Boer RA, Desai AS, Diez M, Drozdz J, Dukat A, Ge J, Howlett JG, Katova T, Kitakaze M, Ljungman CEA, Merkely B, Nicolau JC, O'Meara E, Petrie MC, Vinh PN, Schou M, Tereshchenko S, Verma S, Held C, DeMets DL, Docherty KF, Jhund PS, Bengtsson O, Sjostrand M, Langkilde AM, Committees D-HT Investigators. Dapagliflozin in patients with heart failure and reduced ejection fraction. *N Engl J Med* 2019;**381**:1995–2008
25. Cherney DZI, Dekkers CCJ, Barbour SJ, Cattran D, Abdul Gafor AH, Greasley PJ, Laverman GD, Lim SK, Di Tanna GL, Reich HN, Vervloet MG, Wong MG, Gansevoort RT, Heerspink HJL, DIAMOND Investigators. Effects of the SGLT2 inhibitor dapagliflozin on proteinuria in non-diabetic patients with chronic kidney disease (DIAMOND): a randomised, double-blind, crossover trial. *Lancet Diabet Endocrinol* 2020;**8**:582–93
26. Chertow GM, Vart P, Jongs N, Toto RD, Gorriz JL, Hou FF, McMurray JJV, Correa-Rotter R, Rossing P, Sjöström CD, Stefánsson BV, Langkilde AM, Wheeler DC, Heerspink HJL, DAPA-CKD Trial Committees and Investigators. Effects of dapagliflozin in stage 4 chronic kidney disease. *J Am Soc Nephrol* 2021;**32**:2352–61
27. Nassif ME, Windsor SL, Borlaug BA, Kitzman DW, Shah SJ, Tang F, Khariton Y, Malik AO, Khumri T, Umpierrez G, Lamba S, Sharma K, Khan SS, Chandra L, Gordon RA, Ryan JJ, Chaudhry SP, Joseph SM, Chow CH, Kanwar MK, Pursley M, Siraj ES, Lewis GD, Clemson BS, Fong M, Kosiborod MN. The SGLT2 inhibitor dapagliflozin in heart failure with preserved ejection fraction: a multicenter randomized trial. *Nat Med* 2021;**27**:1954–60
28. Kario K. The sacubitril/valsartan, a first-in-class, angiotensin receptor neprilysin inhibitor (ARNI): potential uses in hypertension, heart failure, and beyond. *Curr Cardiol Rep* 2018;**20**:5
29. Jaffuel D, Nogue E, Berdague P, Galinier M, Fournier P, Dupuis M, Georger F, Cadars MP, Ricci JE, Plouvier N, Picard F, Puel V, Mallet JP, Suehs CM, Molinari N, Bourdin A, Roubille F. Sacubitril-valsartan initiation in chronic heart failure patients impacts sleep apnea: the ENTRESTO-SAS study. *ESC Heart Fail* 2021;**8**:2513–26
30. McMurray JJ, Packer M, Desai AS, Gong J, Lefkowitz MP, Rizkala AR, Rouleau JL, Shi VC, Solomon SD, Swedberg K, Zile MR, Investigators P-H, Committees. Angiotensin-neprilysin inhibition versus enalapril in heart failure. *N Engl J Med* 2014;**371**:993–1004
31. Desai AS, McMurray JJ, Packer M, Swedberg K, Rouleau JL, Chen F, Gong J, Rizkala AR, Brahimi A, Claggett B, Finn PV, Hartley LH, Liu J, Lefkowitz M, Shi V, Zile MR, Solomon SD. Effect of the angiotensin-receptor-neprilysin inhibitor LCZ696 compared with enalapril on mode of death in heart failure patients. *Eur Heart J* 2015;**36**:1990–7
32. Jhund PS, Fu M, Bayram E, Chen CH, Negrusz-Kawecka M, Rosenthal A, Desai AS, Lefkowitz MP, Rizkala AR, Rouleau JL, Shi VC, Solomon SD, Swedberg K, Zile MR, McMurray JJ, Packer M, Investigators P-H Committees. Efficacy and safety of LCZ696 (sacubitril-valsartan) according to age: insights from PARADIGM-HF. *Eur Heart J* 2015;**36**:2576–84
33. Solomon SD, Claggett B, Desai AS, Packer M, Zile M, Swedberg K, Rouleau JL, Shi VC, Starling RC, Kozan Ö, Dukat A, Lefkowitz MP, McMurray JJ. Influence of ejection fraction on outcomes and efficacy of sacubitril/valsartan (LCZ696) in heart failure with reduced ejection fraction: the prospective comparison of ARNI with ACEI to determine impact on global mortality and morbidity in heart failure (PARADIGM-HF) trial. *Circ Heart Fail* 2016;**9**:e002744
34. Gori M, Senni M. Sacubitril/valsartan (LCZ696) for the treatment of heart failure. *Expert Rev Cardiovasc Ther* 2016;**14**:145–53
35. Pelaia C, Armentaro G, Volpentesta M, Mancuso L, Miceli S, Caroleo B, Perticone M, Maio R, Arturi F, Imbalzano E, Andreozzi F, Perticone F, Sesti G, Sciacqua A. Effects of sacubitril-valsartan on clinical, echocardiographic, and polygraphic parameters in patients affected by heart failure with reduced ejection fraction and sleep apnea. *Front Cardiovasc Med* 2022;**9**:861663
36. Kang H, Zhang J, Zhang X, Qin G, Wang K, Deng Z, Fang Y, Chen G. Effects of sacubitril/valsartan in patients with heart failure and chronic kidney disease: a meta-analysis. *Eur J Pharmacol* 2020;**884**:173444
37. Spannella F, Giulietti F, Filipponi A, Sarzani R. Effect of sacubitril/valsartan on renal function: a systematic review and meta-analysis of randomized controlled trials. *ESC Heart Fail* 2020;**7**:3487–96
38. Pontremoli R, Borghi C, Perrone Filardi P. Renal protection in chronic heart failure: focus on sacubitril/valsartan. *Eur Heart J Cardiovasc Pharmacother* 2021;**7**:445–52
39. Yang CC, Sung PH, Chen KH, Chai HT, Chiang JY, Ko SF, Lee FY, Yip HK. Valsartan- and melatonin-supported adipose-derived mesenchymal stem cells preserve renal function in chronic kidney disease rat through upregulation of prion protein participated in promoting PI3K-Akt-mTOR signaling and cell proliferation. *Biomed Pharmacother* 2022;**146**:112551
40. Lu HI, Tong MS, Chen KH, Lee FY, Chiang JY, Chung SY, Sung PH, Yip HK. Entresto therapy effectively protects heart and lung against transverse aortic constriction induced cardiopulmonary syndrome injury in rat. *Am J Transl Res* 2018;**10**:2290–305
41. Ko SF, Sung PH, Yang CC, Chiang JY, Yip HK. Combined therapy with dapagliflozin and entresto offers an additional benefit on improving the heart function in rat after ischemia-reperfusion injury. *Biomed J* 2022;**46**:100546
42. Sheu JJ, Sung PH, Wallace CG, Yang CC, Chen KH, Shao PL, Chu YC, Huang CR, Chen YL, Ko SF, Lee MS, Yip HK. Intravenous administration of iPS-MSC(SPIONs) mobilized into CKD parenchyma and effectively preserved residual renal function in CKD rat. *J Cell Mol Med* 2020;**24**:3593–610
43. Basting T, Lazartigues E. DOCA-salt hypertension: an update. *Curr Hypertens Rep* 2017;**19**:32
44. Zhou Y, Wang S, Li Y, Yu S, Zhao Y. SIRT1/PGC-1alpha signaling promotes mitochondrial functional recovery and reduces apoptosis after intracerebral hemorrhage in rats. *Front Mol Neurosci* 2017;**10**:443
45. Kim SH, Kim H. Inhibitory effect of astaxanthin on oxidative stress-induced mitochondrial dysfunction: a mini-review. *Nutrients* 2018;**10**:1137
46. Halling JF, Pilegaard H. PGC-1alpha-mediated regulation of mitochondrial function and physiological implications. *Appl Physiol Nutr Metab* 2020;**45**:927–36
47. Chen KH, Yang CH, Wallace CG, Lin CR, Liu CK, Yin TC, Huang TH, Chen YL, Sun CK, Yip HK. Combination therapy with extracorporeal shock wave and melatonin markedly attenuated neuropathic pain in rat. *Am J Transl Res* 2017;**9**:4593–606
48. Yuen CM, Yeh KH, Wallace CG, Chen KH, Lin HS, Sung PH, Chai HT, Chen YL, Sun CK, Chen CH, Kao GS, Ko SF, Yip HK. EPO-cyclosporine combination therapy reduced brain infarct area in rat after acute ischemic stroke: role of innate immune-inflammatory response, micro-RNAs and MAPK family signaling pathway. *Am J Transl Res* 2017;**9**:1651–66
49. Yang CC, Sung PH, Chiang JY, Chai HT, Chen CH, Chu YC, Li YC, Yip HK. Combined tacrolimus and melatonin effectively protected kidney against acute ischemia-reperfusion injury. *FASEB J* 2021;**35**:e21661

(Received March 11, 2023, Accepted July 10, 2023)